Effect of steering limit constraints on the performance of variable stiffness laminates

Peeters, Daniël M.J.; Lozano, Gustavo Gonzalez; Abdalla, Mostafa M.

DOI
10.1016/j.compstruc.2017.11.002

Publication date
2018

Document Version
Accepted author manuscript

Published in
Computers & Structures

Citation (APA)
Peeters, D. M. J., Lozano, G. G., & Abdalla, M. M. (2018). Effect of steering limit constraints on the performance of variable stiffness laminates. *Computers & Structures*, *196*, 94-111. https://doi.org/10.1016/j.compstruc.2017.11.002

Important note
To cite this publication, please use the final published version (if applicable).
Please check the document version above.

Effect of Steering Limit Constraints on the Performance of Variable Stiffness Laminates

Daniël M.J. Peeters[a], Gustavo Gonzalez Lozano[b,c], Mostafa M. Abdalla[a]

[a] *Faculty of Aerospace Engineering, Delft University of Technology, Kluyverweg 1, Delft, 2629HS, the Netherlands*
[b] *Airbus Group Innovations, Bristol, UK*
[c] *Manufacturing Department, School of Aerospace, Transport and Manufacturing (SATM), Cranfield University, Bedforshire, UK*

Abstract

A method to optimise the fibre angle distribution of variable stiffness laminates is proposed. The proposed method integrates a fibre angle retrieval step with a fibre angle optimisation procedure. A multi-level approximation approach is used in combination with the method of successive approximations. First, fibre angle retrieval is done by approximating the structural responses based on the optimal stiffness distribution found using lamination parameters. The full fibre angle optimisation is done by updating the approximations based on the current stacking sequence. Next, the actual fibre paths are optimised taking into account the actual size of a tow, and the maximum size of any gap or overlap appearing. The paths are smoothened out using CATIA, and finally NURBS are found that can be sent to the fibre placement machine for manufacturing. It is shown for a bucking optimisation with a stiffness constraint that the number of finite element analyses reduces significantly by starting the optimisation from the optimal stiffness distribution rather than from a user-specified stacking sequence. Next, it is shown that updating the approximations also leads to considerable improvements over fibre angle retrieval. Similar promising results are obtained for a stress optimisation problem.

Keywords: Optimisation, variable stiffness, lamination parameters, manufacturability

A previous version of this paper has been presented at the 20th International conference on composite material, Copenhagen, 19-24 July 2015

Email address: D.M.J.Peeters@tudelft.nl (Daniël M.J. Peeters)

1. Introduction

Today, composite materials are finding increasing application in large commercial aircraft and the first composite-dominated planes like the B-787 or A400M are being built. Traditionally, fibres within a layer have the same orientation, leading to constant stiffness properties. As manufacturing technology has evolved, for example the advent of automated fibre placement machines, the fibre orientation of a layer can be varied continuously leading to varying stiffness properties that can be best tailored for the applied loads. These composites are called variable stiffness laminates (VSL) in the current work.

One of the largest problems in optimising VSL, is taking manufacturability into account. To do this, linearly varying fibre angles are used by many researchers which has given promising, manufacturable, results [1, 2, 3, 4, 5, 6, 7, 8, 9, 10, 11, 12, 13, 14, 15, 16, 17]. The use of linearly varying fibre angle per bay, for stiffened plates, has also been investigated, and again it has been shown that varying the fibre angles leads to better performance [18, 19]. Direct parametrisation of the tow paths using Lagrangian polynomials [20, 21, 22] Lobatto-Legendre polynomials [23, 24], Bezier curves [25, 26, 27], splines [28, 29], B-splines surfaces [30] and NURBS (Non-Uniform Rational B-Splines) [31]. Constant curvature paths have been extensively applied for flat panels and for cylindrical and conical shells [32, 33, 34, 35, 36], as the curvature constraint evaluation is simplified. Large, manufacturable, improvements in buckling load were found, but the result is dependent of the basis functions chosen [31, 37, 20]. Hence, the total potential of VSL has not been exploited due to the pre-specified set of possibilities. Furthermore, most methods assume that the fibres are shifted, meaning a choice had to be made whether gaps or overlaps are allowed during manufacturing [38]. For instance, gaps and overlaps are observed in the cylindrical shells manufactured by Wu et al. [32] and the flat plates manufactured by Tatting and Gürdal[7].

Another approach that leads to manufacturable designs is to align the fibres in the direction of principal stress. This has been shown to reduce stress concentrations, and can also lead to reduced weight using the tailored fibre placement method [39, 40]. Using load paths, or a hybrid combination of load paths and principal stress direction has also been used to design VSLs [41]. Continuous tow shearing is a new manufacturing method, leading to varying fibre angles without

any gaps or overlaps, but with a thickness variation that is coupled with the change in fibre angle [42, 27]. By using a genetic algorithm, coupled with a pattern-search algorithm, or using the infinite strip method, large improvements in structural performance have been shown [43, 44]. A more comprehensive review of optimisation strategies can be found in Ghiasi et al. [45]

For laminate analysis, studies have been conducted on capturing the influence of as-manufactured geometry and features such as gaps, overlaps, tow-drops and variable thickness for the analysis of VSL, by means of 3D FE models [10, 33, 46, 47, 48, 49, 50, 51, 52], analytical methods [53] and experimental tests [50, 54, 55, 56, 57, 58]. Some experiments support the use of overlaps over the tow-drop method for strength and buckling [9, 32, 33, 59]. In addition, experimental tests on flat coupons where carried out by Croft et al. [54] to evaluate the effect of individual manufacturing-induced defects, such as gaps, overlaps and twisted tows. They found that usually defects (gaps or overlaps) that improve one mechanical property also deteriorate another one. Blom et al. [60] proposed a method to optimise the course locations for minimum ply thickness and maximum surface smoothness.

Other manufacturing features are considered in design, such as minimum curvature radius [58, 61, 62, 63, 64, 65, 66] and minimum cut length [57]. A review focused on analysis methods for buckling, failure and vibration was published by Ribeiro et al. [67] and on design for manufacturing by Lozano et al. [68].

To exploit the possibilities of VSL fully, a three-step approach has been developed. The first step is to find the optimal stiffness distribution in terms of the lamination parameters. This is discussed in detail in IJsselmuiden [64, 73]. The second step is to find the optimal manufacturable fibre angle distribution, the focus of this paper [74, 75, 76]. The third step is to retrieve the fibre paths, discussed in Blom [60]. A schematic overview of this approach is shown in Figure 1.

The lamination parameters are optimised in step one of the three-step optimisation approach, which has the disadvantage that a fibre angle retrieval step is needed. Enumeration has been used for constant stiffness laminates to match lamination parameters in terms of fibre angles [77]. If the number of layers gets too high, a layer-wise optimisation approach might have advantages: first, the outer layer(s) are optimised, then the optimisation moves inward [78]. Also a genetic algorithm (GA) is sometimes used for variable stiffness laminates to retrieve fibre angles from the

optimal lamination parameter distribution. Due to the computational cost of a GA, this is limited to a reasonably small number of variables [79, 80]. An approach closely related to the three-step approach is proposed by Wu et al., who first optimise the lamination parameters, followed by a retrieval step using a GA and Lagrangian polynomials. However, no manufacturing constraints are taken into account during the second step, hence the results found are not guaranteed to be manufacturable [81]. Another approach is to try to match the in- and out-of-plane matrices as closely as possible using a combination of a GA and a modified Shepard's interpolation [82]. In other work, a real retrieval step was performed: the fibre angles were optimised using a combination of a GA and a gradient based optimiser to match the optimal stiffness distribution as closely as possible, while obeying a steering constraint [4]. Several authors have employed a streamline analogy, also known as a fluid flow analogy, to compute continuous fibre paths from discrete fibre angles [41, 23, 59, 69, 70, 71, 72].

In this paper, a method is discussed which combines fibre angle retrieval and fibre angle optimisation. First, the angles are retrieved based on the optimal stiffness distribution; next, starting from this fibre angle distribution, fibre angle optimisation is performed. The paper is organised as follows: the optimisation approach is explained in section 2, after which the solution procedure is explained in section 3. The post-processing approach , where the actual fibre paths are found, is explained in section 4. Then, two examples are worked out in more detail: a buckling optimisation example in section 5 and a stress optimisation in section 6. The paper is concluded in section 7.

2. Optimisation approach

In structural optimisation, the minimisation of an objective response (e.g., weight or compliance) subject to performance constraints (e.g., on stresses or displacements) is studied. More generally, the worst case response, for example in the case of multiple load cases, is optimised. Additional constraints not related to structural responses may also be imposed to guarantee certain properties of the design such as manufacturability. The following general problem formulation is considered:

$$\begin{aligned} \min_{x} \quad & \max(f_1, f_2, ..., f_n) \\ s.t. \quad & f_{n+1}, ..., f_m \leq 0 \\ & x \in \mathscr{D} \end{aligned} \tag{1}$$

The functions f_i depend on the design variables; f_1 to f_n denote structural responses that are optimised and f_{n+1} to f_m denote structural responses that are constrained. The feasible region is denoted by $\mathscr{D}$. This problem will be solved using successive approximations: one starts from a certain fibre angle distribution, constructs the approximations based on the optimal stiffness distribution, optimises the approximations and updates the approximations based on the new fibre angles. This is repeated until convergence is reached.

Structural responses, such as buckling loads, stiffness, and strength, are calculated using finite element (FE) analysis. Since each FE analysis is computationally expensive, greater efficiency can be achieved by using structural approximations to reduce the required number of FE analyses [83, 65]. The exact FE response f is approximated in terms of the in- and out-of-plane stiffness matrices A and D and their reciprocals [64]:

$$f^{(1)} \approx \sum_{n=1}^{N} \phi_m : A^{-1} + \phi_b : D^{-1} + \psi_m : A + \psi_b : D + c \tag{2}$$

where the summation takes all nodes n into account, the : operator represents the Frobenius inner product, $A : B = tr(A \cdot B^T)$; ϕ and ψ are calculated from sensitivity analysis [84, 85]. Subscripts m and b denote the membrane and bending parts respectively. This approximation is a generalisation of the linear-reciprocal approximations used in the convex linearisation method [86]. The approximations are convex functions in stiffness space provided that $\phi \geq 0$, a condition that is always satisfied by construction. The free term c equals zero for many types of responses that enjoy homogeneity properties. In this paper, three different structural responses will be used. Their sensitivity analysis is not given in this paper, but is given in previous work: buckling can be found in IJsselmuiden et al. [87], stress in Khani et al. [88], and compliance in IJsselmuiden [64].

In the first step of the three-step approach, the level one approximation, eq. (2), is parametrised

in terms of the lamination parameters. These lamination parameters are defined as:

$$\begin{aligned}(V_1,V_2,V_3,V_4) &= \int_{-\frac{1}{2}}^{\frac{1}{2}} (cos(2\theta(\bar{z})),sin(2\theta(\bar{z})),cos(4\theta(\bar{z})),sin(4\theta(\bar{z})))d\bar{z} \\ (W_1,W_2,W_3,W_4) &= 12\cdot \int_{-\frac{1}{2}}^{\frac{1}{2}} \bar{z}^2\cdot(cos(2\theta(\bar{z})),sin(2\theta(\bar{z})),cos(4\theta(\bar{z})),sin(4\theta(\bar{z})))d\bar{z}\end{aligned} \tag{3}$$

where $\bar{z}$ denotes the normalised z-coordinate. The details of the lamination parameters optimisation are omitted here, they can be found in IJsselmuiden [64]. The outcome of this step is an optimal lamination parameter distribution: on each node the combination of lamination parameters is feasible. Since the lamination parameters describe the stiffness of the laminate, this distribution will be referred to as optimal stiffness distribution in the remainder.

In the second step of the three-step approach the fibre angles are the design variables. Seen as a function of the fibre angles, the level one approximation, eq. (2), no longer has a simple mathematical form and is not generally convex, hence, a level two approximation is constructed based on the level one approximation in terms of the fibre angles:

$$f^{(2)} \approx f_0^{(1)} + g\cdot\Delta\theta + \Delta\theta^T\cdot H\cdot\Delta\theta \tag{4}$$

where $f_0^{(1)}$, g and H denote respectively the function value, gradient and the Gauss-Newton part of the Hessian of the level one approximation at the approximation point. The gradient and Hessian can be calculated starting from

$$f^{(2)}(\theta) = f^{(1)}(s(\theta)) \tag{5}$$

where s contains the components of the stiffness matrices A and D. Differentiating this with respect to the fibre angle θ_i, the i^{th} term of the gradient is found to be

$$g_i = \frac{\partial f^{(1)}}{\partial\theta_i} = \frac{\partial f^{(2)}}{\partial\theta_i} = \frac{\partial f^{(1)}}{\partial s_\alpha}\cdot\frac{\partial s_\alpha}{\partial\theta_i}, \tag{6}$$

where s_α denotes either the in- or out-of-plane stiffness matrix. Differentiating again with respect

to fibre angle θ_j, the ij^{th} term of the Hessian is found to be

$$H_{ij} = \frac{\partial^2 f^{(1)}}{\partial\theta_i \partial\theta_j} = \frac{\partial^2 f^{(1)}}{\partial s_\alpha \partial s_\beta} \cdot \frac{\partial s_\alpha}{\partial \theta_i} \cdot \frac{\partial s_\beta}{\partial \theta_j} + \underline{\frac{\partial f^{(1)}}{\partial s_\alpha} \cdot \frac{\partial^2 s_\alpha}{\partial\theta_i \partial\theta_j}}. \tag{7}$$

Convexity is not guaranteed when using the exact Hessian. Convexity is guaranteed by omitting the underlined part of equation 7, which is not guaranteed to be positive definite, and leaving the positive semi-definite leading term, called the Gauss-Newton part. Only part of the Hessian does not influence the validity of the approximation since a first-order approximation only has to have equal function and gradient values at the approximation point as the approximated function.

While optimising this level two approximation, a steering constraint is introduced to ensure the optimised laminate is manufacturable. In this paper only steering constraints are taken into account during the optimisation: the shape of the part and the manufacturing method also have an influence, but these are not a function of the fibre angle distribution, which is updated in the current work. The steering is defined as the inverse of the minimal steering radius. When the steering radius is too small, the fibres will wrinkle while being laid down. The exact value at which this happens is material and process dependent and hence no value is assumed in the current work. The steering is defined as

$$\varsigma^2 = \frac{2}{\Omega} \cdot \theta^T \cdot L \cdot \theta \tag{8}$$

where L is the standard FEM discretisation of the Laplacian, Ω is the area enclosed, and θ denotes the fibre angles at the nodes of an FE model. If L is taken to be the Laplacian of the complete layer, a global steering constraint is imposed, if the element Laplacian is used, a local steering constraint is imposed. The Laplacian of a triangular element can be calculated using

$$L_{el} = \begin{bmatrix} l1 \cdot l1^T & l1 \cdot l2^T & l1 \cdot l3^T \\ l2 \cdot l1^T & l2 \cdot l2^T & l2 \cdot l3^T \\ l3 \cdot l1^T & l3 \cdot l2^T & l3 \cdot l3^T \end{bmatrix} \tag{9}$$

where l denotes the vector along the edge of an element. To find the Laplacian of the full plate, the different parts have to be assembled according to general finite element routine, in the same way

as the stiffness matrix is assembled.

The global steering constraint is the average steering over the layer, hence this can be loosely interpreted as a measure for the number of gaps and overlaps. The local steering constraint limits the minimal radius of curvature to ensure the machine can lay down the fibre tows without wrinkling. The bound on the local steering ς^U is the inverse of the minimal radius of curvature needed; for example: a maximal steering value of $2m^{-1}$, corresponds to a minimal radius of curvature of $500mm$. When only local steering constraints are used, the complete optimisation problem reads,

$$\begin{aligned} \min_{\theta} \quad & \max(f_1^{(2)}, f_2^{(2)}, ..., f_n^{(2)}) \\ s.t. \quad & f_{n+1}^{(2)}, ..., f_m^{(2)} \leq 0 \qquad i = 1, ..., N \\ & \varsigma_e \leq \varsigma^U \qquad\quad e = 1, ..., E \end{aligned} \tag{10}$$

The details on the fibre angle optimisation, including the steering constraints, can be found in Peeters et al. [65].

3. Solution Procedure

To incorporate the information obtained from the optimal stiffness distribution from step one of the three-step optimisation approach, the sensitivities in the first iteration when using fibre angles as design variables are calculated from the optimal stiffness distribution. This first iteration is called the fibre angle retrieval step. This retrieval step was previously not used, meaning the information of the optimal stiffness distribution was not used. The fibre angle optimisation starts afterwards: the sensitivities are updated based on the current fibre angle distribution to create a new level one approximation which is consequently optimised. The process is repeated until convergence, and is a full fibre angle optimisation. Convergence is defined in terms of the change in objective function: unless specifically mentioned, a $1 \cdot 10^{-3}$ change in objective function is used as the convergence criterion in the current work. It is expected that the fibre angle optimisation after fibre angle retrieval will improve the structural performance: in regions where the stiffness distribution cannot be matched exactly, it is probably advantageous to find an optimal fibre angle distribution rather than approximating the optimal stiffness distribution.

The approximation used for fibre angle optimisation is guaranteed to be convex and separable, meaning every approximation has an optimum and the problem is not computationally expensive. To ensure convergence to a (local) optimum, every step needs to be an improvement (i.e., reduced objective and feasible constraints). When every step is reducing the objective while satisfying all constraints, a local optimum will be found since the objective has physically a minimum. Even though only a local optimum can be guaranteed, previous results starting from different initial guesses showed little variation in performance at the optimum. [65] One possibility to guarantee an improvement step is to make each approximation conservative, meaning it is strictly greater than the function it approximates at the new iterate. This implies that when a finite element analysis is done, the objective will be decreasing and all constraints are satisfied: during the optimisation the approximations of the objective are decreasing, the constraints are satisfied and, since the exact function values are lower than the approximations, the increase in performance is even larger, and feasibility is conserved. To achieve conservative approximations, Svanberg proposed to add a positive function with zero value and gradient at the approximation point to the approximations, referred to as damping function in the remainder [89]. This damping function is scaled with a damping factor which is adjusted to make the approximations conservative. The criterion to accept a new iterate is less stringent: if the new iterate is an improvement, it is accepted, else it is rejected; the damping factor is always updated. The damping function for the first level approximations is chosen as

$$d^{(1)} = \sum_n \left(A_n : A_{n0}^{-1} + D_n : D_{n0}^{-1} + A_n^{-1} : A_{n0} + D_n^{-1} : D_{n0}\right) - 12, \tag{11}$$

where the subscript 0 denotes the value at the approximation point. The damping function for the second level approximations is chosen as [65]

$$d^{(2)}(\theta) = \frac{1}{2}\Delta\theta^T \cdot H_d \cdot \Delta\theta, \tag{12}$$

where $\Delta\theta$ is the change in angles from the approximation point of the level two approximation,

and H_d is a regularisation matrix given by

$$H_d = \frac{1}{s^2}\begin{bmatrix} 1 & -1 & & & \\ -1 & 2 & -1 & & \\ & \ddots & \ddots & & \\ & & -1 & 2 & -1 \\ & & & -1 & 1 \end{bmatrix} + \alpha \begin{pmatrix} 1 & \dots & 1 \\ \vdots & \ddots & \vdots \\ 1 & \cdots & 1 \end{pmatrix}, \tag{13}$$

where s stands for the number of layers in the symmetric part, with α given by

$$\alpha = \frac{\varepsilon \cdot 2 \cdot (s-1)}{s^3}, \tag{14}$$

where ε is a damping factor, usually chosen to be 1. The damping factor of the first level approximation is defined as

$$\zeta_1{}^2 = \sum_n \frac{w_n}{2} \cdot \left(\left(||\phi_{nm} : A_n^{-1}|| + ||\psi_{nm} : A_n|| \right)^2 + \left(||\phi_{nb} : D_n^{-1}|| + ||\psi_{nb} : D_n|| \right)^2 \right). \tag{15}$$

The damping factor for the second level approximation is initialised as

$$\zeta_2{}^2 = \frac{1}{2} \cdot \left(g^T \cdot {H_d}^{-1} \cdot g \right). \tag{16}$$

The damping factor is updated after each iteration using a ratio between the old and optimal damping factor, given by

$$\zeta^* = e^{\frac{f(x^*) - \hat{f}(x^*)}{d}}. \tag{17}$$

The details of the damping function and damping factor can be found in Peeters et al. [65]. The solution procedure is shown in Figure 2, and is explained in algorithm 1.

4. Post processing

The optimal fibres angles distribution has been further processed using the software for manufacturing analysis and optimisation of variable stiffness laminates, FIPAM (Fibre Paths for Man-

Algorithm 1 Solution Procedure

1: start from an initial fibre angle distribution.
2: calculate the sensitivities at the optimal stiffness distribution for the first level approximation $f^{(1)}$.
3: add the damping function $\rho^{(1)} \cdot d^{(1)}$ to the first level approximation.
4: calculate the gradient and Hessian for the second level approximation $f^{(2)}$.
5: add the damping function $\rho^{(2)} \cdot d^{(2)}$ to the second level approximation.
6: apply the steering constraint, build the Lagrangian $\mathscr{L}$ and solve the system.
7: calculate first level approximation $f^{(1)}$ and update damping factor of level two $d^{(2)}$.
8: decide if the new point is accepted: if the first level approximation $f^{(1)}$ is improved, the point is accepted. If the point is accepted, continue, else go back to step 5.
9: check whether the first level approximation $f^{(1)}$ has converged, or the maximum number of iterations is reached. If either of these conditions is met, continue, else return to step 4.
10: perform an FEA and update the damping factor of first level approximation $d^{(1)}$.
11: decide if the new point is accepted: if the FE response has improved, the point is accepted. If the point is accepted, continue, else go back to step 3.
12: perform an FEA and calculate the sensitivities for the first level approximation $f^{(1)}$
13: if FEA has converged, the optimal fibre angle distribution is found, else return to step 3.

ufacturing). This tool enables the automatic generation of fibre paths (i.e., machine trajectories), imposing manufacturing requirements. It is integrated in CATIA V5, where each individual path is modelled considering constraints, such as gaps and overlaps, minimum steering radius, minimum cut length and curve smoothness, to ensure manufacturability of the outcome.

In a first step, the fibre angles for each ply are translated into continuous curves using an iterative procedure where discrete segments are consecutively created following the fibre trajectories. The procedure starts by creating a linear segment from an input starting point. The direction of the segment is obtained by interpolation of the optimal fibre angles at this point. Ordinary Kriging within the library of functions XonGrid Interpolation has been applied as interpolation method, with the power variogram defined as [90]:

$$\gamma(h_{ij}) = \gamma(h_{ij}^{\beta}) \text{ with } 1 \leq \beta \leq 1.99 \tag{18}$$

where h denotes the spatial distance between two random variables (data points), expressed by

$$h_{ij} = (x_i, x_j) = (x_i, x_i + h_{ij}) \tag{19}$$

The length of the segment (i.e., fineness of the discretisation) is a constant value given as input. The endpoint of the segment is the starting point for the consecutive segment, where a new value for the fibre angle is determined using the Kriging interpolant, see Figure 3. This process is repeated iteratively until the segments reach the boundary of the part. From the resulting polylines, splines are modelled and smoothed using CATIA commands (Spline and Curve Smooth) to comply with the minimum turning radius constraint. The details of the smoothing operation are included in Figure 4.

The width of each course (machine pass) can be specified and the proportion between gap and overlap size (coverage) is controlled, shown in Figure 5. The selection of next starting points is done iteratively based on the specified course width. First, a point is chosen, which is contained in a parallel curve to the previous path with an offset equal to the course width. The proportion of gaps and overlaps between the original reference and the one created from the new starting point are computed. The position of the starting point is tuned until the required coverage is met. This procedure is summarised in algorithm 2. The ply design resulting from following the optimal angles may present large gaps and overlaps affecting the manufacturability of the laminate.

Algorithm 2 Modelling of continuous reference curves from vector map of fibre orientations

1: Select starting point.
2: Create segment following optimal angle at point.
3: Interpolate angle at end of segment.
4: Create new segment with the interpolated angle and the end of the previous segment as start point
5: If curve is not finished (cover the surface) then go to step 3
6: Join the segments to create a polyline or store the points of start/end of segments to fit a curve.
7: Curve fitting. Options: 1) using the reference points as inputs, create cubic Bezier curves through two consecutive reference points, which are joined;2) create a general Bezier curve of n-degree using the reference points as control points; 3) use the spline command of CATIA (creation of a NUPBS).
8: Curve smoothing: measure minimum radius of curvature and smooth the curve in case it does not comply with the minimum turning radius.
9: Select next starting point and go to step 2. The selection of the starting points is done iteratively, by choosing points contained in a parallel curve to a previous reference with an offset equal to the course width. The position of the starting point is tuned to comply with the defined proportion between gaps and overlaps.

In a second step, new fibre paths for manufacturing are modelled approaching the previously defined paths. Choosing one curve as starting path, the method consists of defining a feasible region where the next path should be placed to comply with the specifications on course width, maximum gap and maximum overlap. The new path is created within this region trying to approach the trajectory of the closest reference curve from the first step. To create this manufacturable path, several equally distributed points are created on the current fibre path (initially, it is the starting path). The number of points or distance between points is defined at the start of the process. Distances are measured from these points to the target reference, normally to the current fibre path. The minimum distance to the target reference is used to calculate how many fibre paths would fit between the source current path and the target according to the course width. If there is no space between the current path and the target reference to create a path, then that reference is ignored and the next nearest reference is used. The feasible region where the fibre path must be contained to comply with the manufacturing constraints is defined by two curves: one, a parallel curve to the current fibre path with a distance equal to the course width minus the maximum overlap allowance, and two, a parallel offset of the course width plus the allowable gap, shown in Figure 6. A set of control points are generated by offsetting the points created on the current path at a distance normal to the path on the part surface (i.e., on the distance lines between current path and reference). These points must lie inside the feasible region. For that purpose, the following formulas have been used:

$$
\begin{aligned}
&\text{If} \quad \tfrac{MaxDistance-MinDistance}{PathsInBetween} / \geq (MaxGap+MaxOverlap) \quad \textit{then} \\
&\quad ControlPoint(i) = \big((MaxGap+MaxOverlap)\tfrac{Distance(i)-MinDistance}{MaxDistance-MinDistance}^{\,weight} + \\
&\quad CourseWidth-MaxOverlap\big)\cdot p \\
&\text{Else if} \quad \tfrac{MaxDistance-MinDistance}{pathsInBetween} \leq MaxGap \quad \textit{then} \\
&\quad ControlPoint(i) = \big(\tfrac{MaxDistance-MinDistance}{pathsInBetween}\cdot\tfrac{Distance(i)-MinDistance}{MaxDistance-MinDistance}^{\,weight} \\
&\quad +Coursewidth\big)\cdot p \\
&\text{Else} \quad ControlPoint(i) = \big(\tfrac{MaxDistance-MinDistance}{pathsInBetween}\cdot(\tfrac{Distance(i)-MinDistance}{MaxDistance-MinDistance}^{\,weight}-1) \\
&\quad +Coursewidth+maxGap\big)\cdot p
\end{aligned}
\tag{20}
$$

where $MaxDistance$ and $MinDistance$ denote the maximum and minimum distance between the current path and the reference, respectively. $Distance(i)$ is the distance to the reference of point(i) on the current path. $MaxGap$ and $MaxOverlap$ are the manufacturing constraints specified for maximum acceptable gaps and overlaps; $PathsInBteween$ is the number of fibre paths that will be created between the current path and the reference; p is the path number; and $Weight$ is a factor to decide whether giving more importance to the current path or the reference. The $Weight$ value is normally set to 1. Values lower than 1 will result in the fibre path closer to the reference and higher values result in a path closer to the current path. As generally gaps are preferred over overlaps, the formulas prioritise the presence of gaps within the allowable limits; meaning that if possible, it will eliminate overlaps by using the maximum size of gaps permitted.

A spline is fitted through the calculated control points. The path smoothing algorithm described for the first step is also used here to ensure the created spline satisfies the constraint on minimum turning radius. A compromise between minimising angular deviation from the optimal trajectories and reducing gaps, overlaps and tow drop-offs is sought. The process is repeated until completion of the ply, using the new path as current path and the closest curve from the set of reference curves from the first step as new target to approach. The solution procedure is further explained in algorithm 3.

Algorithm 3 Solution procedure to model fibre paths for manufacturing based on target approach method

1: Input values
Set of reference curves
Manufacturing constants: gap and overlap allowance, number of tows, tow width, gap between tows, minimum turning radius, maximum angle deviation allowed (optional)
Settings: Accuracy of distance measurements (number of points on curve) and priority (in case not all constraints can be satisfied)
2: Select starting path (= current path)
3: Sort references according to distance to starting path and side with respect to it
4: Define direction of movement (side)
5: Find nearest reference. If Current path intersects reference (and intersections are not enabled) then, go to next reference; else, select that reference as target
6: Measure minimum distance to target reference. Calculate Number of paths in between: PathsInBetween= Round(MinimumDistance/CourseWidth). If PathsInBetween = 0, go to step 16; else:
7: Calculate origin and end of current path where distances will be calculated. Distances are measured normal to current path
8: Create points on current path equally distributed along the active segment
9: Compute distances to reference measured normal to current path
10: Create control points by offsetting the points on the current path along the distance lines between current path and reference using formulas described in eq. (20) (objective: approach reference and stay in feasibility region)
11: Fit a spline curve through the control points
12: Split and extrapolate curve (fibre path) to cover the surface
13: Check maximum curvature and smooth new curve if necessary
14: If maximum angle deviation constraint is used, constraints on gaps and overlaps may not be fulfilled. Analyse individual gaps/overlaps between current path and new fibre path and tune position of fibre path if necessary to satisfy the constraint that is prioritised (either maximum gap or maximum overlap)
15: Make Current path = new fibre path, and go to step 6
16: Calculate if ply is completed.
If reference = last reference on one side then, enable intersections (to ensure coverage of the ply) and go to step 5
If Side has been completed then: select Starting path = Current path; change orientation (do the other side) and go to step 5
If all references have been used then end

5. Buckling optimisation

The first example is a singly-curved plate under compression. The buckling load of the plate is optimised with the constraint that the axial stiffness should be at least as much as that of a quasi-isotropic laminate of the same thickness. To have a minimisation problem, the inverse buckling load is considered during the optimisation. Furthermore, to avoid mode jumping, the inverse of the lowest two buckling loads are simultaneously considered using a min-max formulation. The compliance constraint is set to avoid unstable post-buckling behaviour, which is dependent on the overall in-plane stiffness. The buckling performance is mainly dependent on the out-of-plane stiffness and the relative change in in-plane stiffness distribution over the plate [91]. The plate is 600 by 400mm, with a sine-shaped height difference, which is maximal 75mm in the middle. The left edge cannot move in x-direction, while the right edge is loaded with a unit compressive force while this edge is to remain straight (i.e., all nodes on the right edge have the same displacement in x-direction). All edges are constrained to not move out-of-plane, and one node is extra constrained in y-direction to suppress rigid body modes. A graphical representation can be seen in figure 7. The material properties are as follows: $E_1 = 154GPa$, $E_2 = 10.8GPa$, $G_{12} = 4.02GPa$ and $\nu_{12} = 0.317$. The balanced layers are assumed to be next to each other, no thickness variation is taken into account. The physical laminate has 36 layers in total, but since symmetry and balance are imposed, only 9 *design layers* are part of the optimisation problem. The optimisation problem can be formulated as

$$\begin{aligned} \min_{\theta} \quad & \max(f_1^{(2)}, f_2^{(2)}) \\ s.t. \quad & f_3^{(2)} \leq 0 \qquad i = 1,...,N \\ & \varsigma_e \leq \varsigma^U \qquad e = 1,...,E \end{aligned} \tag{21}$$

where $f_1^{(2)}$ denotes the inverse of the first buckling mode, $f_2^{(2)}$ denotes the inverse of the second buckling mode, and $f_3^{(2)}$ denotes the compliance minus the compliance of the quasi-isotropic laminate. The steering constraint is kept general since multiple values will be used. During the optimisation, the level two approximations are used, hence the superscript (2).

A mesh convergence study indicated that a sufficiently fine mesh is to use 24 elements in y-direction, and 36 in x-direction, leading to 1728 triangular elements and 925 nodes in the model

used during optimisation. Due to the symmetry of the problem, only a quarter of the plate will be used during the optimisation, reducing the number of nodes in the optimisation to 247, and the number of elements to 432. The complete model is used for the FE analysis and sensitivity calculation.

In the first step, the optimal stiffness distribution is found, which has buckling loads of 2.2432 and 2.4656 times the lowest QI buckling load while the stiffness is 1.0001 times the QI stiffness. The QI material is defined as all lamination parameters equal to zero; no lay-up is known. Since the laminate is balanced and symmetric, the only non-zero lamination parameters are V_1, V_3, W_1, and W_3. The optimal lamination parameters are shown in Figure 8.

5.1. Influence of initial fibre angle retrieval

The optimisation will be performed twice to assess the computational advantages of the fibre angle retrieval step. The first time, the initial level one approximation is calculated at a user-specified initial fibre angle distribution. The second time, the initial level one approximation is calculated at the optimal stiffness distribution. When starting from the sensitivities of the optimal stiffness distribution, the first iteration is a fibre angle retrieval step. Five level one iterations are allowed, following previous work done by the authors [65]. Only a local steering constraint of $3m^{-1}$, corresponding to a minimal radius of curvature of $333mm$, is used for this investigation. In the following, the buckling load and stiffness values are normalised with respect to the corresponding values of a QI laminate of the same thickness.

The results are shown in Table 1. The initial fibre angle distribution is assumed to be uniform for all layers and nodes. The initial angle is shown in the first column. The optimal buckling load, and number of FEAs used when no retrieval step is applied are shown in the second and third columns. The optimal buckling load, and number of FEAs used with fibre angle retrieval activated are shown in the fourth and fifth columns. The difference in optimal buckling load and FEAs used between the two optimisation strategies are shown in the last two columns. The stiffness is not shown in Table 1 to save space, but it was always equal to the QI stiffness, or slightly higher, also only the critical buckling load is shown; the second buckling load was always close to it but not identical. It can be seen from Table 1 that the influence of the initial fibre angles is

limited: a maximum change of 1.2 % is observed. The solution procedure seems to be robust to initial conditions. When using fibre angle retrieval, the number of FEAs always decreases, in most cases it is halved. The difference in optimal buckling load due to the different initial sensitivities is negligible, less then 1%, and may be explained by the stopping criterion in a gradient-based algorithm.

Observing the convergence history, shown in Figure 9, the largest improvement is seen to be made in the first level one step, which is the retrieval step. When fibre angle retrieval is used, less iterations are needed to 'fine-tune' the design. This could be because in the first step the stiffness distribution is already getting to the best one based on the optimal stiffness, while when starting from the initial fibre angle distribution, there is more fine-tuning to be done.

It is interesting to inspect the convergence of the level two optimisation. To check this, an FEA is done after each level two update until convergence is reached. This is done for an initial fibre angle of $1, 10$ and 20° as can be seen in Figure 10. For some cases convergence is established fairly quickly and the 5 inner iteration limit imposed earlier is adequate. For the case of a 10° initial angle the convergence is slower and it is possible that more inner iterations are beneficial. The reason the convergence is not monotonous (i.e., constantly decreasing response) is that during level two updates, level one approximations are monitored and are guaranteed to decrease. It can happen that the level two updates wander out of the range of validity of level one approximations leading to non-monotone convergence of the FEA results.

A maximum improvement over QI of 60% is found when fibre angle retrieval is used on its own. This means that about 30% of the improvement is lost compared to the optimum in terms of lamination parameters. This is more than what Wu et al. found [81], but can be explained by the manufacturing constraints that are imposed in the current work. The lamination parameters after the retrieval step can be seen in Figure 11. Comparing to Figure 8, it can be seen the optimal lamination parameters are not matched exactly, but the general trends are similar. After updating the approximations and converging the full fibre angle optimisation, a 76% improvement is found. The lamination parameters after the fibre angle optimisation can be seen in Figure 12. Comparing to the lamination parameters after the fibre angle retrieval step, the differences are not large, but these small changes do lead to a considerable improvement in performance. Thus, the best optimi-

sation strategy seems to be to combine the fibre angle retrieval and angle optimisation. This way a better performance is achieved while keeping the cost, in terms of number of FEAs, low.

The post-processing described in section 4 has been applied to the fibre angles from optimisation to control the gaps and overlaps. The objective was to minimise the amount and size of overlaps, keeping the size of gaps below 2 mm (a commonly used acceptance criteria in industry) and a minimum steering radius of 333 mm. Minimising these manufacturing defects comes at the expense of increasing the angular deviation from the structural optimal. Results are shown for plies 1 and 7, when starting to count from the outside, and imposing a constraint on the maximum allowable angle deviation in Table 2 and Figure 13. If no angle deviation is allowed, the fibre path design obtained corresponds to the closest paths that approximate the optimal fibre angles, meaning the reference paths from step 1 of the post-processing approach.

Significant improvements are obtained when this constraint is relaxed. Increasing the allowable fibre angle deviation to 5° results in a reduction in the amount of overlaps, 86.0% reduction for ply 1 as can be seen in Figure 13b, and 57.6% for ply 7, see Figure 13e, with respect to the reference curves created by interpolation of the optimal fibre angles, shown in Figure 13a and 13d, respectively. In addition, the gap area for both plies is larger for the paths for manufacturing than the reference paths. That is because gaps below 2 mm are acceptable and the paths for manufacturing use more efficiently the acceptable gap size to reduce the overlaps.

Removing the constraint on angle deviation provides an upper limit to the angle deviation necessary to nearly eliminate the presence of overlaps. The paths and analysis of gaps and overlaps are depicted in Figure 13c for ply 1 and Figure 13f for ply 7. Note that the curves represent the centrelines of the fibre paths, where the angular deviation constraint is applied. As the paths have a width, there is a fibre deviation between the centreline and the inner and outer boundaries. Therefore, an additional angle deviation error is expected when computing the manufacturing fibre angles at the data points. Also the interpolation method introduces a small error in the form of angular deviation from the optimal. The analysis of gaps and overlaps is performed assuming no tow-dropping. Overlaps can be removed by dropping the tows, although triangular gaps will appear.

5.2. Influence of manufacturing constraints

The influence of manufacturing constraints on how close the optimal stiffness response can be approached is investigated. First, the optimisation is performed for different levels of the maximum local steering, there is no constraint on the global steering. The results, for a local steering of $1m^{-1}$ up to $5m^{-1}$, are shown in Table 3, where the maximum local steering is shown in the first column, the optimal buckling load with only fibre angle retrieval is shown in the second column, the optimal buckling loads and stiffness are shown in columns three to five. The sixth column lists the number of FEAs needed, the seventh column indicates the improvement obtained by full fibre angle optimisation over only fibre angle retrieval, and the last column lists the difference in performance with respect to the stiffness optimum. Note that the level two optimisation in the fibre angle retrieval step was allowed to converge fully to ensure a fair comparison between the results with and without full fibre angle optimisation.

The higher the allowed steering, the higher is the improvement in buckling load. Furthermore, it seems that the difference obtained by performing fibre angle optimisation after the retrieval step diminishes. This is due to the better fit that can be obtained at higher steering values.

The Pareto front trading off manufacturability versus structural performance is shown in Figure 14: the minimum turning radius represents manufacturability and the buckling load represents performance. The Pareto front is not convex which is typical of the highly non-convex buckling optimisation problem. It seems that initially large performance improvements can be made by decreasing the minimum steering radius of curvature; the improvements become gradually less significant for tighter radii. The response does seem to converge to the stiffness optimum as expected. This shows that when manufacturing constraints are relaxed, the optimum in terms of lamination parameters can almost be matched, certainly much closer than the values reported in Wu et al.

As discussed earlier, the local steering constraint is imposed to guarantee a minimum radius of curvature. This is not the only manufacturing consideration; gaps/overlaps due to fibre divergence/convergence may develop. These are considered manufacturing defects and it is desirable to minimise them. Detailed prediction of gaps and overlaps requires full simulation of the fibre-placement process. Embedding a full simulation in the optimisation process, as is discussed in

section 4 and shown in Figure 13, would not be feasible. This is especially due to the additional geometric freedom, not related to the fibre angle distribution, is available to the designer to space the fibres in a way that best avoids gaps and overlaps. During the optimisation, we propose to use the global steering as a surrogate measure of the extent of local defects in the laminate. A reasonable value for the local steering, 4 m^{-1} corresponding to a minimal radius of curvature of 250mm, is selected and fixed. The upper bound on global steering is varied to investigate the effect on optimal performance.

The results are shown in Table 4, where the global steering constraint is shown in the first column, the optimal buckling load after fibre angle retrieval is shown in the second column. The optimal buckling loads and stiffness are shown in columns three to five. The number of FEAs is shown in the sixth column, the difference obtained by full angle optimisation is shown in the seventh column while the last column indicates the difference with respect to the optimal stiffness design. The lowest value used for global steering is small enough to be considered as the optimal straight-fibre, constant stiffness, laminate. Up to 55% improvement in the buckling load can be achieved by manufacturable steered laminates. The difference between fibre angle retrieval and full optimisation is mostly around 20% supporting our earlier observations about the improvement of fibre angle optimisation over only fibre angle retrieval.

6. Strength optimisation

The second example problem is the taken from Khani et al. [88]. A plate with a circular cut-out loaded in tension is optimised for strength. The plate is 400 by 400mm, with a large circular cut-out with a diameter of 200mm at the centre. The plate is simply supported all around, with all edges constrained to remain straight. A graphical representation can be seen in Figure 15. After taking the symmetry into account, the plate was discretised into 217 triangular elements with 132 nodes. The material stiffness properties are as follows: $E_1 = 142.9GPa$, $E_2 = 10.3GPa$, $G_{12} = 7.2GPa$ and $\nu_{12} = 0.27$. The failure is defined using the conservative omni-strain envelope [92, 88, 93]. The total laminate has a thickness of 4.6mm, meaning there are 24 layers. As in the previous example, the laminate is assumed the be balanced and symmetric, leading to 6 design

layers. The optimisation problem can be formulated as

$$\begin{aligned} \min_{\theta} \quad & \max(f_1^{(2)}, ..., f_n^{(2)}) \\ s.t. \quad & \varsigma_e \leq \varsigma^U \qquad e = 1, ..., E \end{aligned} \tag{22}$$

where f_1 up to f_n denote the stress at the different nodes, and the steering constraint is again kept general since multiple values are used. During the optimisation, the level two approximations are used, hence the superscript (2).

The load is chosen such that the QI design has a minimum factor of safety of 1. As in the previous example, the QI laminate is defined by all lamination parameters equal to zero. When performing the optimisation in terms of the lamination parameters, the optimal design has a minimum factor of safety of 1.944. Only the effect of the local steering constraint will be investigated. The optimisation will be performed for straight fibres, by setting the maximum local steering to $0.01m^{-1}$, and for local steering bounds from 1 to $3m^{-1}$. The results are shown in Table 5, where the local steering constraint is shown in the first column. The maximum failure index after angle retrieval and after optimisation are shown in the second and third column, the fourth column gives the number of FEAs needed to get to the optimum, the difference from angle retrieval due to full optimisation is shown in column six, the last column indicates the difference with respect to the optimum stiffness distribution.

The small number of FEAs needed for the straight-fibre laminate stands out: only 4. Although the approximations are only updated four times, there is a clear advantage in updating them. The large increase in safety factor after the fibre angle retrieval is due to the bad matching in the vicinity of the hole: updating the approximations makes sure the optimal fibre angle is found, as opposed to a suboptimal lamination parameter match. The number of FEAs is low due to the limited design space: no steering is allowed, thus not much 'fine-tuning' can be done.

When steering is allowed, the increase in safety factor is more significant. This comes at the cost of significantly more FEAs. Since steering is allowed, a wider design space is available to the optimiser, and a lot of 'fine-tuning' can be done. If the convergence criterion is chosen to be $3 \cdot 10^{-3}$ instead of $1 \cdot 10^{-3}$, fewer FEAs will be needed, but at the expense of reduced optimal

performance. The results are shown in Table 6. This table has the same layout as Table 5 with one column added where the difference with respect to the tighter convergence criterion is given.

What really stands out is that even with a relatively limited steering of $3m^{-1}$, one can already get within 4% of the optimal stiffness distribution. This can be explained by the relatively low load redistribution that has to be done for the stress optimisation. For buckling optimisation, all the load is redistributed to the sides, while for the strength, the load is gently nudged away from the cut-out, possibly because of the geometry: the cut-out is large compared to the total size of the plate.

To see what is happening in terms of the stiffness distribution, the V_1 and V_3 distribution are shown in Figure 16. The optimal stiffness distribution found is shown at the top, the lamination parameters after the fibre angle retrieval step are shown in the middle, and the optimal fibre angle distribution is shown in the bottom. A local steering constraint of $3m^{-1}$ is used for the fibre angle retrieval and optimisation. In the top figures, it can be seen there is a lot of difference in stiffness from one point to the next, which causes the stiffness distribution after the fibre angle retrieval step to be very far away from the optimal, not knowing what places should be matched more accurately. When looking at the stiffness distribution for the fibre angle optimum, it can be seen that the stiffness change is smoother, and the sides and middle are matched exactly, while the part in between looks completely different. Although the difference in stiffness distribution is very large, the factor of safety only differs by 3%: the stiffness optimisation allows very large changes in stiffness from one point to the next for a small increase in performance, while this is constrained in the fibre angle optimisation.

7. Conclusion

A method to optimise the fibre angle distributions of variable stiffness laminates is proposed. The proposed method integrates a fibre angle retrieval step with the fibre angle optimisation procedure. The fibre angles are retrieved using the approximation based on the optimal stiffness distribution, meaning there is a direct connection between the optimum in terms of the stiffness and the optimisation of the fibre angles. Due to a steering constraint, which limits the rate of change in fibre angles, the stiffness distribution cannot, in general, be matched exactly. Hence, fibre angle

optimisation is performed, using successive approximations, after the fibre angle retrieval step, until convergence is reached. Finally, a novel post-processing step is performed to find the exact fibre path definitions. Two examples are used to demonstrate the approach. The first example shown is a singly-curved plate under compression, optimised for buckling with a stiffness constraint. The second example is a square plate with a circular hole in the centre under tension, optimised for maximum strength. The results indicate a strong trade-off between manufacturability, measured by the bound on steering, and performance.

The results show that by incorporating a fibre angle retrieval step, the number of FEAs goes down significantly, usually it is halved, compared to starting from a user-specified initial stacking sequence. While the fibre angle retrieval leads to improved numerical efficiency, the results indicate that fibre angle retrieval in itself is not sufficient to obtain the best performance. Further full fibre angle optimisation steps, in the buckling example, led on average to 15-20% improvement in performance over fibre angle retrieval. The strength optimisation example showed that even larger improvements are possible by performing full fibre angle optimisation, almost 35% on average. The best strategy seems to be to combine fibre angle retrieval and angle optimisation. This way a better performance is achieved while limiting the number of FE analyses.

Next to the fibre angle distribution optimisation, also a fibre path optimisation has been performed. This bridges the gap from the optimised fibre angle distribution to manufacturing. During the fibre path generation the tow width and a maximum size of gaps and overlaps is taken into account. The fibre paths are smoothed using CATIA and the resulting NURBS can be sent to a fibre placement machine for manufacturing.

Overall, integration of fibre-angle retrieval in the full fibre angle optimisation process reduces the computational cost. Compared to only performing fibre angle retrieval, the performance has significantly increased. This gain in efficiency and performance will allow designers to study the trade-off between manufacturability and performance carefully and to select the most promising design(s) depending on the relative importance of both considerations.

8. Acknowledgements

This work is supported by the CANAL (CreAting Non-conventionAl Laminates) Project, part of the European Union Seventh Framework Program.

[1] Lopes, C., Gürdal, Z., and Camanho, P., "Tailoring for strength of composite steered-fibre panels with cutouts," *Composites Part A: Applied Science and Manufacturing*, Vol. 41, No. 12, 2010, pp. 1760 – 1767.

[2] Gürdal, Z., Tatting, B., and Wu, C., "Variable stiffness composite panels: Effects of stiffness variation on the in-plane and buckling response," *Composites Part A: Applied Science and Manufacturing*, Vol. 39, No. 5, 2008, pp. 911 – 922.

[3] Hyer, M. W. and Charette, R. F., "Use of curvilinear fiber format in composite structure design," *AIAA Journal*, Vol. 29, No. 6, 1991, pp. 1011–1015.

[4] van Campen, J. M., Kassapoglou, C., and Gürdal, Z., "Generating realistic laminate fiber angle distributions for optimal variable stiffness laminates," *Composites Part B: Engineering*, Vol. 43, No. 2, 2012, pp. 354 – 360.

[5] Stodieck, O., Cooper, J., Weaver, P., and Kealy, P., "Improved aeroelastic tailoring using tow-steered composites," *Composite Structures*, Vol. 106, 2013, pp. 703–715. Cited By 7.

[6] Ungwattanapanit, T. and Baier, H., "Postbuckling analysis and optimization of stiffened fuselage panels utilizing variable-stiffness laminates," in "Congress of the International Council of the Aeronautical Sciences, ICAS [29., 2014, St. Petersburg]," , 2014.

[7] Tatting, B. F., Gürdal, Z., and Jegley, D., "Design and manufacture of elastically tailored tow placed plates," .

[8] Tatting, B. F. and Gürdal, Z., "Analysis and design of variable stiffness composite cylinders," .

[9] Lopes, C., Gürdal, Z., and Camanho, P., "Variable-stiffness composite panels: Buckling and first-ply failure improvements over straight-fibre laminates," *Computers and Structures*, Vol. 86, No. 9, 2008, pp. 897 – 907. Composites.

[10] Lopes, C., *Damage and failure of non-conventional composite laminates*, Ph.D. thesis, Delft University of Technology, 2009.

[11] Zamani, Z., Haddadpour, H., and Ghazavi, M., "Curvilinear fiber optimization tools for design thin walled beams," *Thin-Walled Structures*, Vol. 49, No. 3, 2011, pp. 448–454.

[12] Haddadpour, H. and Zamani, Z., "Curvilinear fiber optimization tools for aeroelastic design of composite wings," *Journal of fluid structures*, Vol. 33, 2012, pp. 180–190.

[13] Stanford, B., Jutte, C. V., and Wu, C., "Aeroelastic benefits of tow steering for composite plates," *composite structures*, Vol. 118, 2014, pp. 416–422.

[14] Alhajahmad, A., Abdalla, M., and Gürdal, Z., "Optimal design of tow-placed fuselage panels for maximum strength with buckling considerations," *Journal of aircraft*, Vol. 47, 2010, pp. 775–782.

[15] Akhavan, H. and Ribeiro, P., "Geometrically non-linear periodic forced vibrations of imperfect laminates with curved fibres by the shooting method," *Composites Part B: Engineering*, Vol. 109, 2017, pp. 286–296.

[16] Samukham, S., Raju, G., and Vyasarayani, C., "Parametric instabilities of variable angle tow composite laminate under axial compression," *Composite structures*, Vol. 166, 2017, pp. 229–238.

[17] Haldar, A., Reinoso, J., Jansen, E., and Rolfes, R., "Thermally induced multistable configurations of variable stiffness composite plates: Semi-analytical and finite element investigation," *Composite structures*.

[18] Liu, W. and Butler, R., "Buckling optimization for composite panels with elastic tailoring," in "49th AIAA/ASME/ASCE/AHS/ASC Structures, Structural Dynamics and Materials Conference," , 2008.

[19] Coburn, B., Wu, Z., and Weaver, P., "Buckling analysis of stiffened variable angle tow panels," *Composite structures*, Vol. 111, No. 1, 2014, pp. 259–270.

[20] Wu, Z., Weaver, P. M., Raju, G., and Kim, B. C., "Buckling analysis and optimisation of variable angle tow composite plates," *Thin-Walled Structures*, Vol. 60, No. 0, 2012, pp. 163 – 172.

[21] Wu, Z., Weaver, P., and Raju, G., "Postbuckling optimisation of variable angle tow composite plates," *Composite structures*, Vol. 103, 2013, pp. 34–42.

[22] Guimaraes, T., Castro, S., Rade, D., and Cesnik, C., "Panel Flutter Analysis and Optimization of Composite Tow Steered Plates," in "58th AIAA/ASMe/ASCE/AHS/SC Structures, Structural Dynamics, and Materials Conference," , 2017.

[23] Alhajahmad, A., Abdalla, M., and Z., G., "Design Tailoring for Pressure Pillowing Using Tow-Placed Steered Fibers," *Journal of aircraft*, Vol. 45, 2008, pp. 630–640.

[24] Demasi, L., Santarpia, E., R, C., Biagini, G., and Vannucci, F., "Zig-Zag and Layer wise theories for Variable-Stiffness composite laminates based on the Generalized Unified Formulation," in "58th AIAA/ASMe/ASCE/AHS/SC Structures, Structural Dynamics, and Materials Conference," , 2017.

[25] Dems, K. and Winiewski, J., "Optimal design of fibre-reinforced composite disks," *Journal of theoretical and applied mechanics*, Vol. 47, 2009, pp. 515–535.

[26] Parnas, L., Oral, S., and Ceyhan, U., "Optimum design of composite structures with curved fiber courses," *Composite science and technology*, Vol. 63, 2003, pp. 1071–1082.

[27] Kim, B., Potter, K., and Weaver, P., "Continuous tow shearing for manufacturing variable angle tow composites," *Composites, Part A: Applied Science and Manufacturing*, Vol. 43, No. 8, 2012, pp. 1347–1356.

[28] Honda, S. and Narita, Y., "Natural frequencies and vibration modes of laminated composite plates reinforced with arbitrary curvilinear fiber shape paths," *Journal of sound and vibrations*, Vol. 331, 2012, pp. 180–191.

[29] Honda, S., Narita, Y., and Sasaki, K., "Maximizing the Fundamental Frequency of Laminated Composite Plates with Optimally Shaped Curvilinear Fibers," *Journal of system design and dynamics*, Vol. 3, 2009, pp. 867–876.

[30] Montemurro, M. and Catapano, A., "On the effective integration of manufacturability constraints within the multi-scale methodology for designing variable angle-tow laminates," *composite structures*, Vol. 161, 2017, pp.

145–159.

[31] Nagendra, S., Kodiyalam, S., Davis, J. E., and Parthasarathy, V. N., "Optimization of Tow Fiber Paths for Composite Design," in "36th AIAA/American Society of Mechanical Engineers/American Society of Civil Engineers/American Helicopter Society/ Society for Composites Structures, Structural Dynamics, and Materials Conference," , 1995.

[32] Wu, K., Tatting, B., Smith, B., Stevens, R., Occhipinti, G., and Swift, J., "Design and manufacturing of tow-steered composite shells using fiber placement," in "50th AIAA/ASMe/ASCE/AHS/SC Structures, Structural Dynamics, and Materials Conference," , 2009.

[33] Fayazbakhsh, K., Nik, M., Pasini, D., and Lessard, L., "Defect layer method to capture effect of gaps and overlaps in variable stiffness laminates made by Automated Fiber Placement," *Composite Structures*, Vol. 97, 2013, pp. 245 – 251,
doi:http://dx.doi.org/10.1016/j.compstruct.2012.10.031.

[34] Blom, A., Stickler, P., and Gürdal, Z., "Optimization of a composite cylinder under bending by tailoring stiffness properties in circumferential direction," *composites part B Engineering*, Vol. 41, 2010, pp. 157–165.

[35] Nik, M., Fayazbakhsh, K., Pasini, D., and Lessard, L., "Optimization of variable stiffness composites with embedded defects induced by Automated Fiber Placement," *Composite Structures*, Vol. 107, 2014, pp. 160 – 166,
doi:http://dx.doi.org/10.1016/j.compstruct.2013.07.059.

[36] Akbarzadeh, A., Arian Nik, M., and Pasini, D., "The role of shear deformation in laminated plates with curvilinear fiber paths and embedded defects," *composite structures*, Vol. 118, 2014, pp. 217–227.

[37] van den Brink WM, Vankan, W., and Maas, R., "Buckling optimized variable stiffness laminates for a composite fuselage window section," in "28th international congress of the aeronautical sciences," , 2012.

[38] Gürdal, Z., Tatting, B., and Wu, K., "Tow-Placement Technology and Fabrication Issues for Laminated Composite Structures," in "46th AIAA/ASME/ASCE/AHS/ASC Structures, Structural Dynamics and Materials Conference," American Institute of Aeronautics and Astronautics, 2005.

[39] Crothers, P., Drechsler, K., Feltin, D., Herszberg, I., and Kruckenberg, T., "Tailored fibre placement to minimise stress concentrations," *Composites Part A: Applied Science and Manufacturing*, Vol. 28, No. 7, 1997, pp. 619 – 625.

[40] Richter, E., Uhlig, K., Spickenheuer, A., Bittrich, L., Maäder, E., and Heinrich, G., "thermoplastic composite parts based on online spun commingled hybrid yarns with continuous curvilinear fibre patterns," in "16th European Conference on Composite Materials," , 2014.

[41] Tosh, M. and Kelly, D., "On the design, manufacture and testing of trajectorial fibre steering for carbon fibre composite laminates," *Composites Part A: Applied Science and Manufacturing*, Vol. 31, No. 10, 2000, pp. 1047 – 1060.

[42] Kim, B., Potter, K., and Weaver, P., *Multi-tow shearing mechanism for high-speed manufacturing of variable angle tow composites*, 2012. Venice, IT.

[43] Groh, R. and Weaver, P., "Mass Optimization of Variable Angle Tow, Variable Thickness Panels with Static Failure and Buckling Constraints," in "56th AIAA/ASME/ASCE/AHS/ASC Structures, Structural Dynamics and Materials Conference," , 2015.

[44] Liu, W. and Butler, R., "Buckling Optimization of Variable-Angle-Tow Panels Using the Infinite-Strip Method," *AIAA Journal*, Vol. 51, No. 6, 2013, pp. 1442–1449.

[45] Ghiasi, H., Fayazbakhsh, K., Pasini, D., and Lessard, L., "Optimum stacking sequence design of composite materials Part II: Variable stiffness design," *Composite Structures*, Vol. 93, No. 1, 2010, pp. 1 – 13.

[46] Fagiano, C., *Computational modeling of tow-placed composite laminates with fabrication features*, Ph.D. thesis, Delft University of Technology, 2010.

[47] Kärger, L. and Kling, A., "As-built FE simulation of advanced fibre placement structures based on manufacturing data," *composite structures*, Vol. 100, 2013, pp. 104–112.

[48] Rhead, a. T., Dodwell, T., and Butler, R., "The effect of tow gaps on compression after impact strength of AFP laminates," in "15th European conference on composite materials," , 2012.

[49] Rhead, a. T., Dodwell, T., and Butler, R., "The effect of tow gaps on compression after impact strength of robotically laminated structures," *computational materials continua*, Vol. 35, 2013, pp. 1–16.

[50] Dang, T., Hallett, S., Kim, B., Le Cahain, Y., Butler, R., and Liu, W., "Modelling of as manufactured geometry for prediction of impact and compression after impact behaviour of variable angle tow laminates," *journal of composite materials*, Vol. 0, 2014, pp. 1–16.

[51] Blom, A., Lopes, C., Kromwijk, P., Gürdal, Z., and Camanho, P., "A theoretical model to study the influence of tow-drop areas on the stiffness and strength of variable-stiffness laminates," *journal of composite materials*, Vol. 43, 2009, pp. 403–425.

[52] O, F., Mayugo, J., Lopes, C., Gascons, N., Turon, A., and Costa, J., "Variable-stiffness composite panels: As-manufactured modeling and its influence on the failure behavior," *composites part B: Engineering*, Vol. 56, 2014, pp. 660–669.

[53] Lucas, D., Van Tooren, M., and Elham, A., "Stiffness Corrections for Overlaps and Gaps in Steered Composite Panel Optimization," in "58th AIAA/ASMe/ASCE/AHS/SC Structures, Structural Dynamics, and Materials Conference," , 2017.

[54] Croft, K., Lessard, L., Pasini, D., Hojjati, M., Chen, J., and Yousefpour, A., "Experimental study of the effect of automated fiber placement induced defects on performance of composite laminates," *Composites Part A: Applied Science and Manufacturing*, Vol. 42, No. 5, 2011, pp. 484 – 491, doi:http://dx.doi.org/10.1016/j.compositesa.2011.01.007.

[55] O, F., Mayugo, J., Lopes, C., Gascons, N., Turon, A., and Costa, J., "Variable-stiffness composite panels: Defect

tolerance under in-plane tensile loading," *composites part A: Applied science and manufacturing*, Vol. 63, 2014, pp. 21–31.

[56] Falco, O., Lopes, C., Mayugo, J., Gascons, N., and Renart, J., "Effect of tow-drop gaps on the damage resistance and tolerance of Variable-Stiffness Panels," *composite structures*, Vol. 116, 2014, pp. 94–103.

[57] Blom, A., Stickler, P., and Gürdal, Z., "Design and manufacture of a variable-stiffness cylindrical shell," in "SAMPE Europe: 30th international conference," , 2009.

[58] Peeters, D. and Abdalla, M., "Effect of Steering Constraints on the Performance of Variable Stiffness Laminates," in "20th international conference on composite materials, Copenhagen," , 2015.

[59] Mills, A., Patel, Z., Frost, M., and DellAnno, G., "Resin transfer moulding of highly loaded carbon fibre composite aircraft spars using novel fabrics and tow placement techniques," *SAMPE journal*, Vol. 43, 2007, pp. 67–72.

[60] Blom, A. W., Abdalla, M. M., and Gürdal, Z., "Optimization of course locations in fiber-placed panels for general fiber angle distributions," *Composites Science and Technology*, Vol. 70, No. 4, 2010, pp. 564 – 570.

[61] C, W., "Analysis of tow-placed, variable-stiffness laminates," *Virginia Polytechnic Institute and State University*.

[62] Waldhart, C., Gürdal, Z., and Ribbens, C., "Analysis of tow placed, parallel fiber, variable stiffness laminates," in "37th AIAA/ASMe/ASCE/AHS/SC Structures, Structural Dynamics, and Materials Conference," , 1996.

[63] Pilaka, V., *Design of realistic variable stiffness laminates - a gradient-based optimizer for retrieving fiber orientation angles with average curvature constraints from lamination parameter distributions*, M.Sc. thesis, Delft University of Technology, 2010.

[64] IJsselmuiden, S. T., *Optimal design of variable stffness composite structures using lamination parameters*, Ph.D. thesis, Delft University of Technology, 2011.

[65] Peeters, D., Hesse, S., and Abdalla, M., "Stacking sequence optimisation of variable stiffness laminates with manufacturing constraints," *Composite Structures*, Vol. 125, 2015, pp. 596 – 604.

[66] Irisarri, F.-X., Peeters, D., and Abdalla, M., "Optimisation of Ply Drop Order in Variable Stiffness Laminates," *Composite Structures*, pp. –,
doi:http://dx.doi.org/10.1016/j.compstruct.2016.05.076.

[67] Ribeiro, P., Akhavan, H., Teter, A., and Warmiski, J., "A review on the mechanical behaviour of curvilinear fibre composite laminated panels," *Jurnal of composite materials*, Vol. 48, 2014, pp. 2761–2777.

[68] Lozano, G. G., Tiwari, A., Turner, C., and Astwood, S., "A review on design for manufacture of variable stiffness composite laminates," *Proceedings of the Institution of Mechanical Engineers, Part B: Journal of Engineering Manufacture*, Vol. 230, No. 6, 2016, pp. 981–992,
doi:10.1177/0954405415600012.

[69] Tosh, M. and Kelly, D., "Fibre steering for a composite C-beam," *Composite structures*, Vol. 53, 2001, pp. 133–141.

[70] Gliesche, K., Hübner, T., and Orawetz, H., "Application of the tailored fibre placement (TFP) process for a local reinforcement on an open-hole tension plate from carbon/epoxy laminates," *Composite science and technology*, Vol. 63, 2003, pp. 81–88.

[71] Charan, R., Renault, T., Ogale, A., and Bagchi, A., "Automated fiber reinforced composite prototypes," in "5th International conference on rapid prototyping," , 1994.

[72] van Campen, J., Kassapoglou, C., and Gürdal, Z., "Design of fiber-steered variable-stiffness laminates based on a given lamination parameters distribution," in "52nd AIAA/ASMe/ASCE/AHS/SC Structures, Structural Dynamics, and Materials Conference," , 2011.

[73] Peeters, D., van Baalen, D., and Abdalla, M., "Combining topology and lamination parameter optimisation," *Structural and Multidisciplinary Optimization*, pp. 1–16.

[74] Autio, M., "Determining the real lay-up of a laminate corresponding to optimal lamination parameters by genetic search," *Structural and Multidisciplinary Optimization*, Vol. 20, No. 4, 2000, pp. 301–310.

[75] Setoodeh, S., Blom, A., Abdalla, M., and Gürdal, Z., "Generating Curvilinear Fiber Paths from Lamination Parameters Distribution," in "47th AIAA/ASME/ASCE/AHS/ASC Structures, Structural Dynamics, and Materials Conference," American Institute of Aeronautics and Astronautics, 2006.

[76] van Campen, J. and Gürdal, Z., "Retrieving Variable Stiffness Laminates from Lamination Parameters Distribution," in "50th AIAA/ASME/ASCE/AHS/ASC Structures, Structural Dynamics, and Materials Conference," American Institute of Aeronautics and Astronautics, 2009.

[77] Honda, S., Narita, Y., and Sasaki, K., "Discrete Optimization for Vibration Design of Composite Plates by Using Lamination Parameters," *Advanced Composite Materials*, Vol. 18, No. 4, 2009, pp. 297–314.

[78] Narita, Y., "Layerwise optimization for the maximum fundamental frequency of laminated composite plates," *Journal of Sound and Vibration*, Vol. 263, No. 5, 2003, pp. 1005 – 1016. Arthur W. Leissa 70th Birthday Issue.

[79] Liu, S., Hou, Y., Sun, X., and Zhang, Y., "A two-step optimization scheme for maximum stiffness design of laminated plates based on lamination parameters," *Composite Structures*, Vol. 94, No. 12, 2012, pp. 3529 – 3537.

[80] Raju, G., White, S., Wu, Z., and Weaver, P., *Optimal Postbuckling Design of Variable Angle Tow Composites using Lamination Parameters*, American Institute of Aeronautics and Astronautics, 2015.

[81] Wu, Z., Raju, G., and Weaver, P. M., "Framework for the Buckling Optimization of Variable-Angle Tow Composite Plates," *AIAA Journal*, Vol. 53, No. 12, 2015, pp. 3788–3804.

[82] "Stacking Sequence Optimization of Blended Composites using a Modified Shepard's Method and Stacking Sequence Tables," *composite structures*.

[83] de Wit, A. and van Keulen, F., "Numerical Comparison of Multi-Level Optimization Techniques," in "48th AIAA/ASME/ASCE/AHS/ASC Structures, Structural Dynamics, and Materials Conference," American Institute of Aeronautics and Astronautics, 2007.

[84] Haftka, R. and Gürdal, Z., *Elements of Structural Optimization*, Contributions to Phenomenology, Springer Netherlands, 1992.

[85] Kumar, V., Lee, S.-J., and German, M., "Finite element design sensitivity analysis and its integration with numerical optimization techniques for structural design," *Computers and Structures*, Vol. 32, No. 34, 1989, pp. 883 – 897.

[86] Fleury, C., "CONLIN: An efficient dual optimizer based on convex approximation concepts," *Structural optimization*, Vol. 1, No. 2, 1989, pp. 81–89.

[87] Ijsselmuiden, S. T., Abdalla, M. M., and Gürdal, Z., "Optimization of Variable-Stiffness Panels for Maximum Buckling Load Using Lamination Parameters," *AIAA Journal*, Vol. 48, No. 1, 2010, pp. 134–143.

[88] Khani, A., IJsselmuiden, S., Abdalla, M., and Grdal, Z., "Design of variable stiffness panels for maximum strength using lamination parameters," *Composites Part B: Engineering*, Vol. 42, No. 3, 2011, pp. 546 – 552.

[89] Svanberg, K., "a class of globally convergent optimization methods based on conservative convex separable approximations," *Siam J. optim*, Vol. 2, 2002, pp. 555–573.

[90] Deglo de Besses, B., "XonGrid Interpolation," `http://xongrid.sourceforge.net/`. Accessed: 2015-02-02.

[91] Rahman, T., Ijsselmuiden, S., Abdalla, M., and Jansen, E., "Postbuckling analysis of variable stifness composite plates using a finite element-based perturbation method," *International Journal of Structural Stability and Dynamics*, Vol. 11, No. 04, 2011, pp. 735–753, doi:10.1142/S0219455411004324.

[92] Ijsselmuiden, S. T., Abdalla, M. M., and Gürdal, Z., "Implementation of Strength-Based Failure Criteria in the Lamination Parameter Design Space," *AIAA Journal*, Vol. 46, No. 7, 2008, pp. 1826–1834.

[93] Tsai, S. W. and Melo, J. D. D., "An invariant-based theory of composites," *Composites Science and Technology*, Vol. 100, No. 0, 2014, pp. 237 – 243.

[94] Kassapoglou, C., *Design and analysis of composite structures*, John Wiley and Sons, Ltd, 2010.

[95] Tsai, S. W. and Hahn, H., *Introduction to composite materials*, Technomic, Westport, 1989.

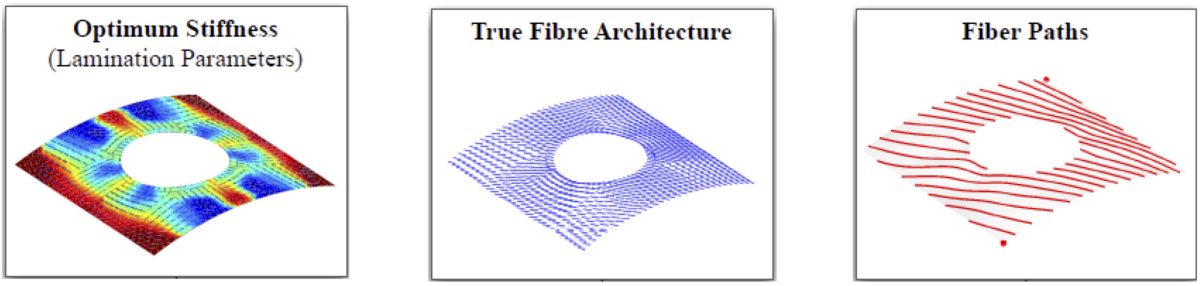

Figure 1. schematic overview of the three-step optimisation approach [64]

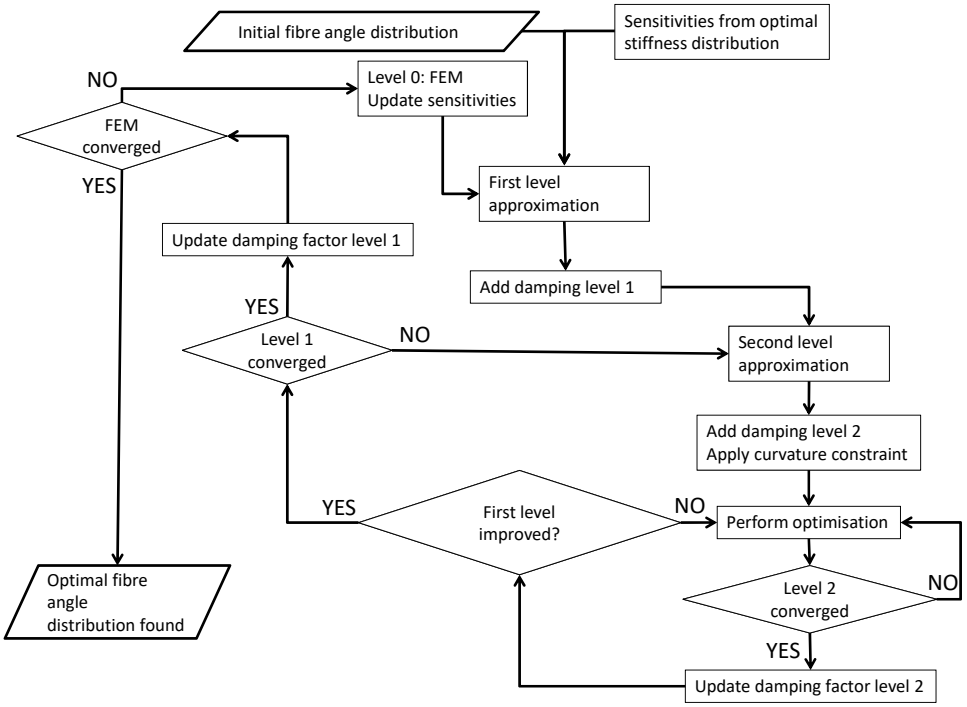

Figure 2. schematic overview of the code for a single optimisation step

Table 1. Overview of the results using different initial sensitivities

initial fibre angles [deg]	optimal buckling load without fibre angle retrieval [-]	number of FEAs without fibre angle retrieval retrieval	optimal buckling load with fibre angle retrieval [-]	number of FEAs with fibre angle retrieval retrieval	difference in buckling load	difference FEAs used
0.1	1.7574	14	1.7696	8	+ 0.7 %	- 6
1	1.7620	21	1.7671	5	+ 0.3 %	- 16
10	1.7608	13	1.7486	8	- 0.7 %	- 5
20	1.7628	11	1.7645	5	+ 0.1 %	- 6

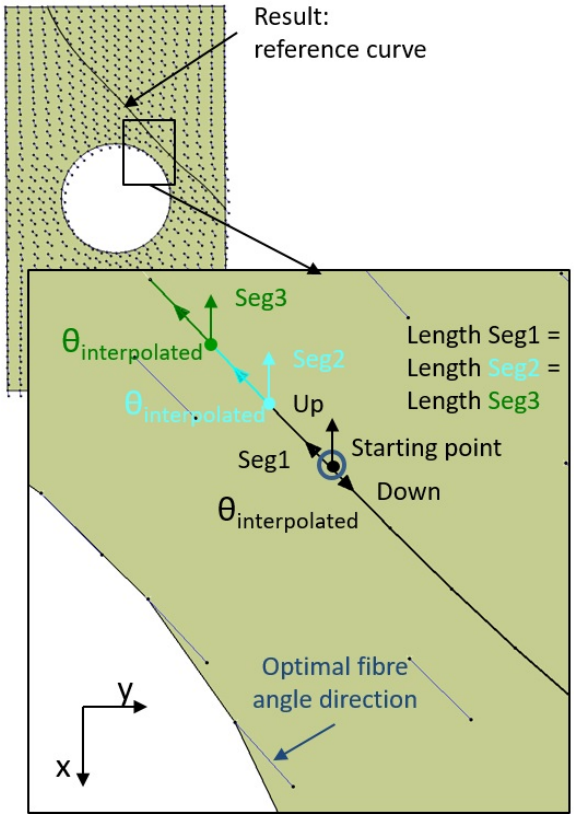

Figure 3. Description of algorithm to create continuous fibre paths using Kriging multivariate interpolation method.

Table 2. Analysis of gaps, overlaps and angular deviations of paths for manufacturing of ply 1 and ply 7

	ply 1	ply 1	ply 1	ply 7	ply 7	ply 7
Constraint: maximum allowable angle deviation [deg]	0	5	not applied	0	5	not applied
Maximum overlap size (mm)	14.00	8.73	0.21	16.78	14.75	0.53
Maximum gap size (mm)	1.99	2.09	2.09	2.08	2.09	2.11
Total gap area (%)	0.41	3.10	4.11	1.06	2.51	4.82
Total overlap area (%)	20.46	2.87	0.0033	32.56	13.80	0.0029
Average of angular deviation from optimal [deg]	1.11	3.57	5.26	0.94	4.22	9.43
Standard deviation of angular deviation from optimal [deg]	0.93	1.84	3.71	0.60	1.84	6.80
Maximum angular deviation [deg]	6.15	10.91	17.65	3.32	7.67	29.47

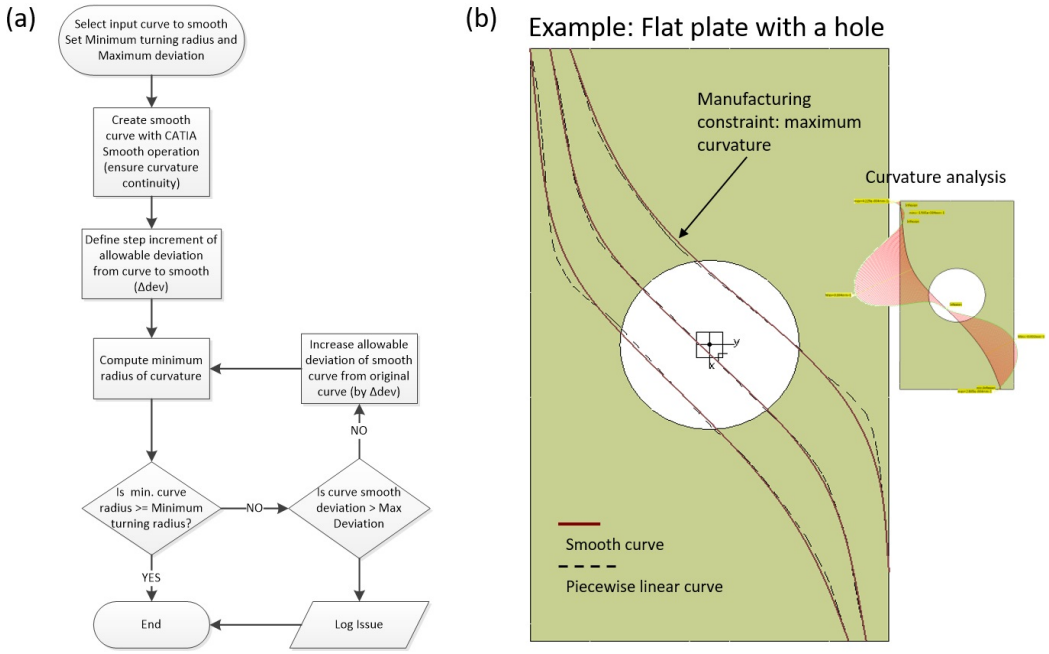

Figure 4. (a) Flowchart of curve smoothing approach to comply with minimum turning radius constraint; (b) Example of smoothing operation on a flat plate with a hole.

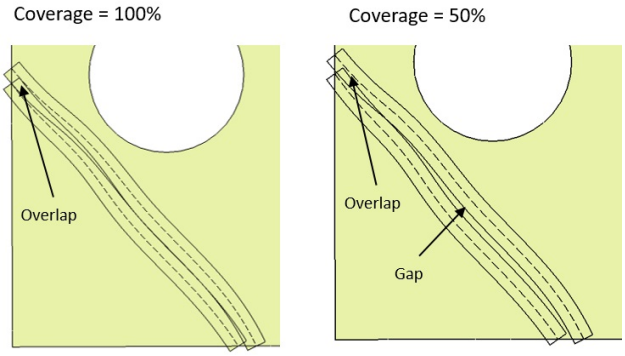

Figure 5. Generation of two reference curves on a plate with a hole with course width = 25.4mm and different input values for gap/overlap proportion (coverage).

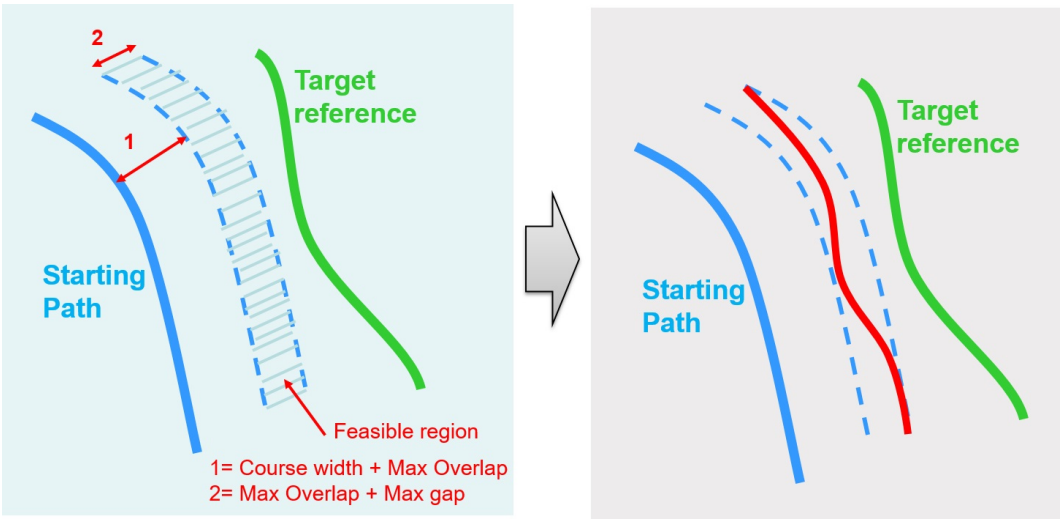

Figure 6. Process rationale to create fibre paths for manufacturing approaching reference curves.

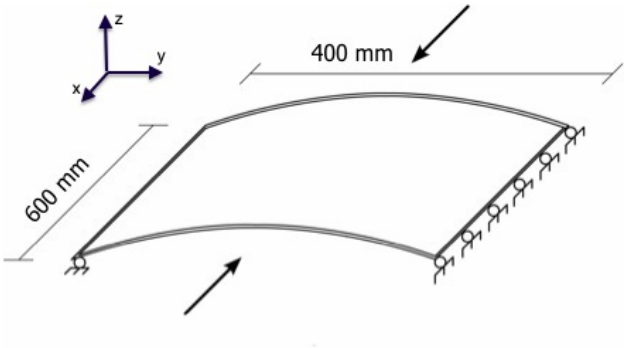

Figure 7. Load case and boundary conditions for the bucking optimisation

Table 3. Overview of the results using different local steering constraints

maximum local steering $[m^{-1}]$	optimal buckling load after fibre angle retrieval [-]	optimal buckling load 1 [-]	optimal buckling load 2 [-]	optimal stiffness [-]	number of FEAs	difference w.r.t. optimum after fibre angle retrieval	difference w.r.t. optimal stiffness distribution
1	1.1210	1.3731	1.3735	1.0012	4	+ 22.5 %	- 38.8%
2	1.2894	1.5749	1.5752	1.0005	5	+ 22.1 %	- 29.8%
3	1.4867	1.7474	1.7474	1.0008	5	+ 17.5 %	- 22.1%
4	1.6024	1.8846	1.8852	1.0010	4	+ 17.6 %	- 16.0%
5	1.7550	1.9830	1.9835	1.0007	5	+ 13.0 %	- 11.6%

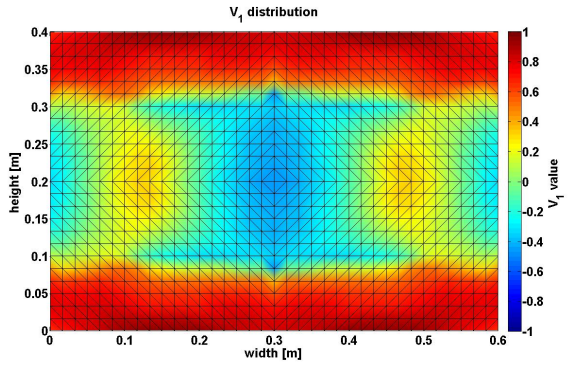

(a) V_1 distribution

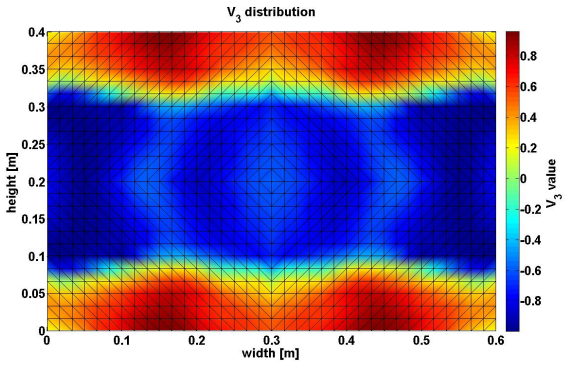

(b) V_3 distribution

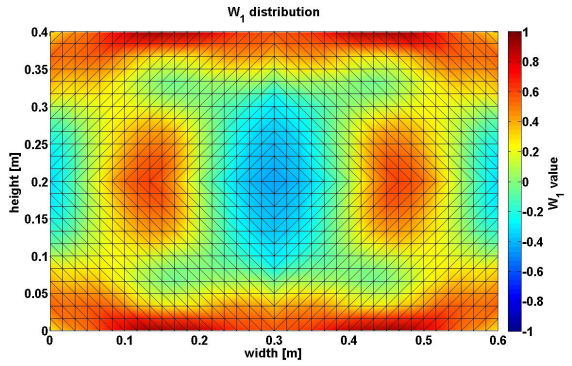

(c) W_1 distribution

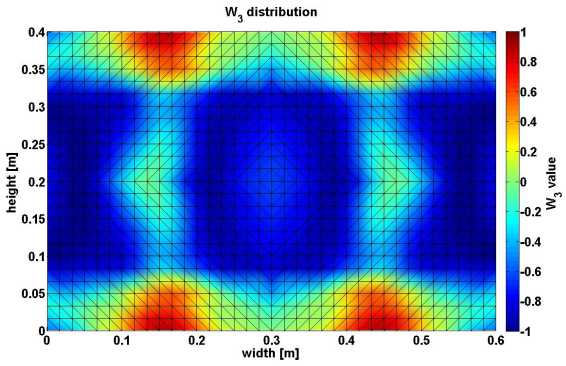

(d) W_3 distribution

Figure 8. optimal lamination parameters for the buckling optimisation

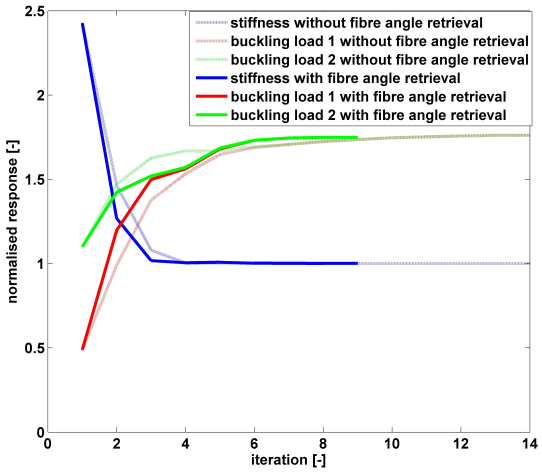

Figure 9. convergence history with and without initial fibre angle retrieval step

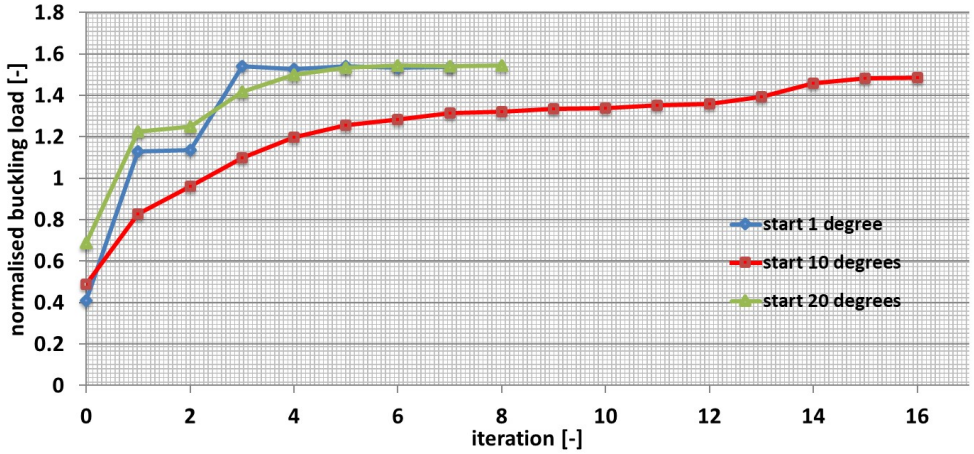

Figure 10. FE response after each level 2 optimisation (during fibre angle retrieval)

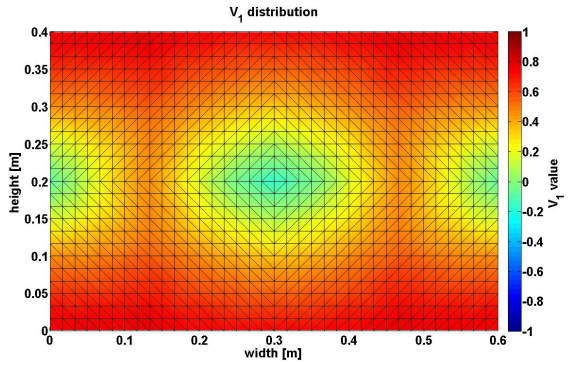

(a) V_1 distribution

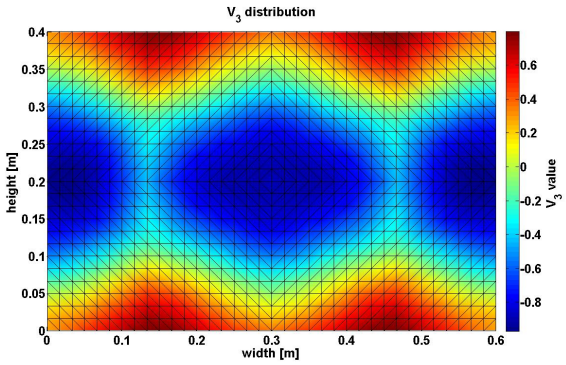

(b) V_3 distribution

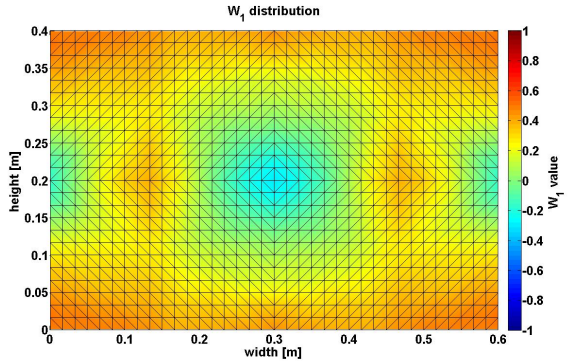

(c) W_1 distribution

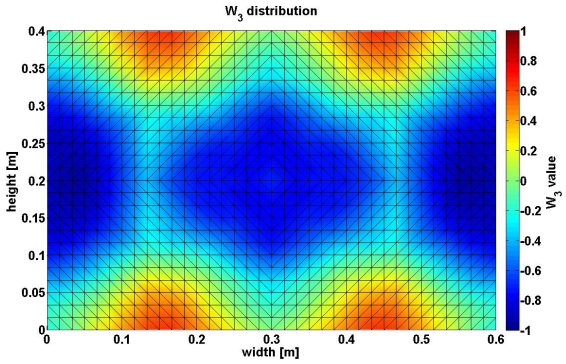

(d) W_3 distribution

Figure 11. lamination parameters after the fibre angle retrieval step for the buckling optimisation

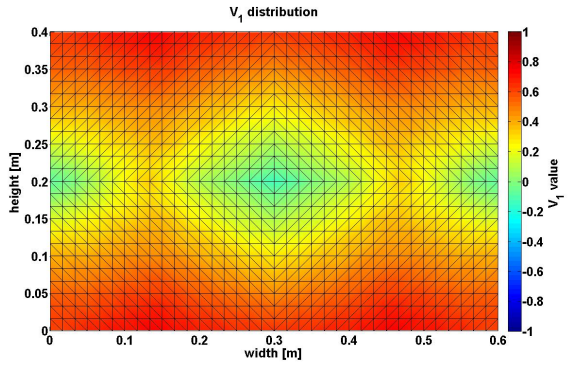

(a) V_1 distribution

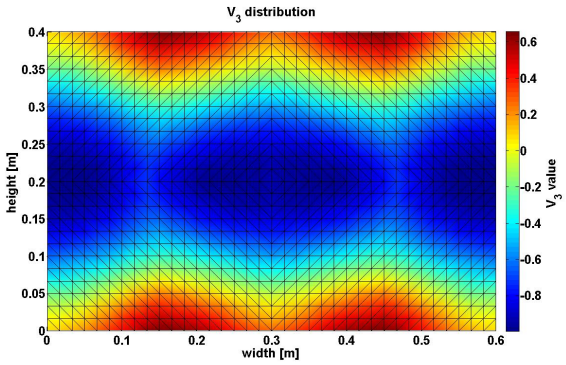

(b) V_3 distribution

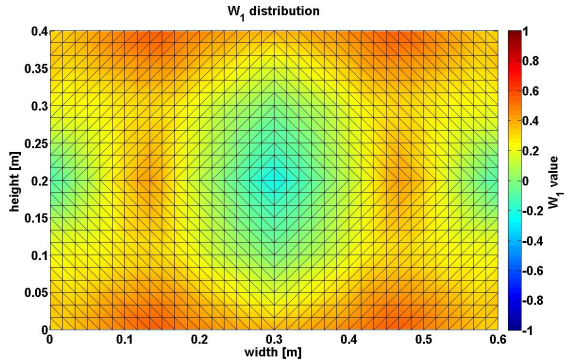

(c) W_1 distribution

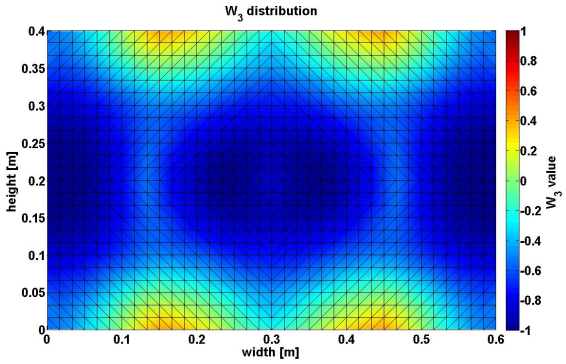

(d) W_3 distribution

Figure 12. lamination parameters after the fibre angle optimisation for the buckling optimisation

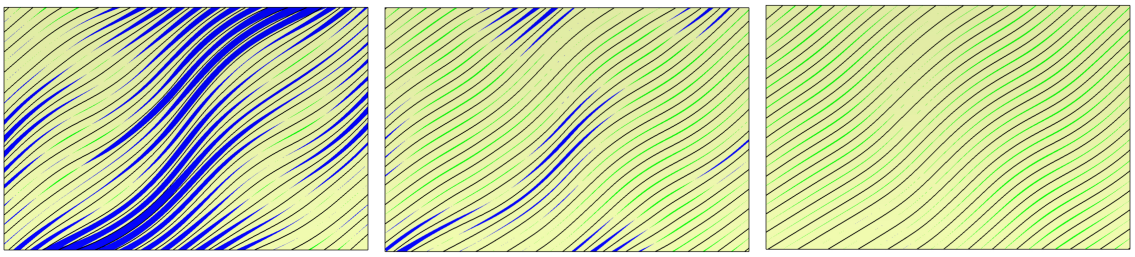

(a) Ply 1; maximum angle deviation = 0°

(b) Ply 1; maximum angle deviation = 5°

(c) Ply 1; angle deviation not constrained

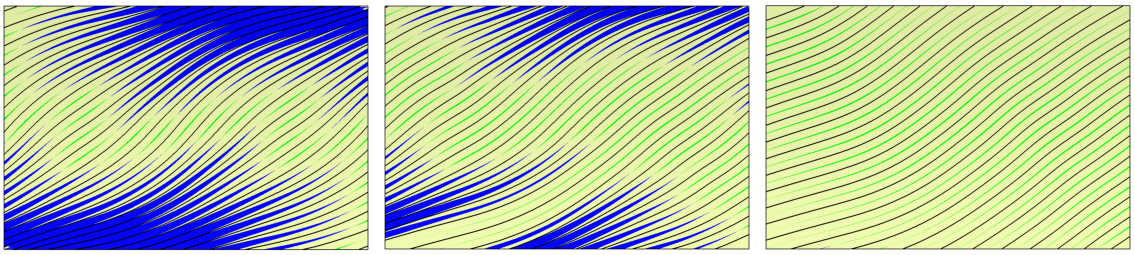

(d) Ply 7; maximum angle deviation = 0°

(e) Ply 7; maximum angle deviation = 5°

(f) Ply 7; angle deviation not constrained

Figure 13. Analysis of gaps and overlaps of fibre paths for manufacturing with minimum steering radius = 333 mm and maximum gap size = 2 mm (overlaps represented in blue and gaps in green)

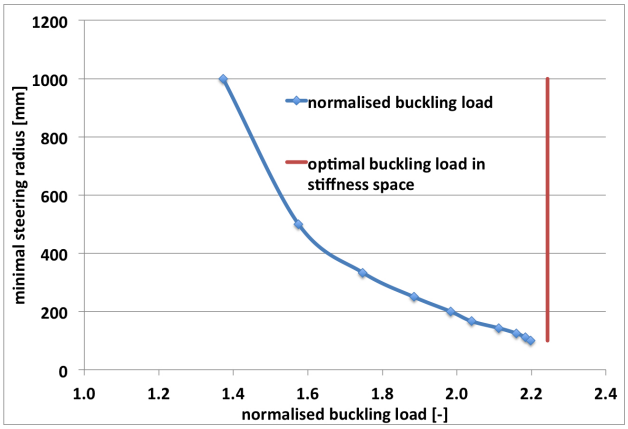

Figure 14. normalised buckling load versus the minimal steering radius

Table 4. Overview of the results using different global steering constraints

maximum global steering $[m^{-1}]$	optimal buckling load after fibre angle retrieval [-]	optimal buckling load 1 [-]	optimal buckling load 2 [-]	optimal stiffness [-]	number of FEAs	difference w.r.t. optimum after fibre angle retrieval	difference w.r.t. optimal stiffness distribution
0.01	1.0307	1.2132	1.2132	1.1067	6	+ 17.7%	- 45.9%
0.5	1.0519	1.2888	1.2888	1.0011	5	+ 22.5%	- 42.6%
1	1.1274	1.3992	1.3999	1.0011	4	+ 24.1%	- 37.6%
1.5	1.2292	1.5192	1.5196	1.0007	5	+ 23.6%	- 32.3%
2	1.3532	1.6330	1.6333	1.0007	5	+ 20.7%	- 27.2%
2.5	1.4819	1.7436	1.7441	1.0006	6	+ 17.7%	- 22.3%
3	1.5724	1.8034	1.8046	1.0005	4	+ 14.7%	- 19.6%
3.5	1.0181	1.8467	1.8481	1.0013	8	+ 81.4%	- 17.7%
4	1.6024	1.8846	1.8852	1.0010	4	+ 17.6 %	- 16.0%

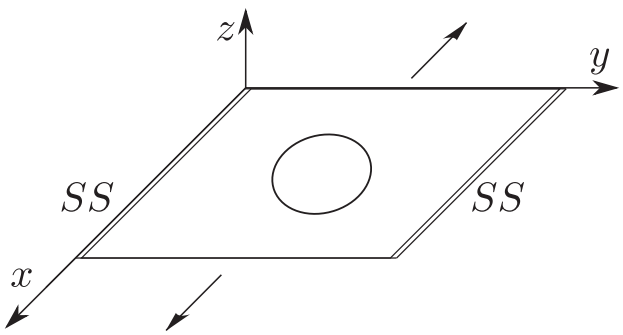

Figure 15. Load case and boundary conditions for the strength optimisation

Table 5. Overview of the results using different local steering constraints using $1 \cdot 10^{-3}$ as stopping criterion

maximum local steering $[m^{-1}]$	minimum factor of safety after fibre angle retrieval [-]	optimal factor of safety [-]	number of FEAs	difference w.r.t. optimum after fibre angle retrieval	difference w.r.t. optimal stiffness distribution
0.01	1.288	1.578	4	+ 22.5 %	- 18.8 %
1	1.345	1.811	10	+ 34.6 %	- 6.8 %
2	1.357	1.830	12	+ 34.9 %	- 5.9 %
3	1.395	1.869	15	+ 34.0 %	- 3.9 %

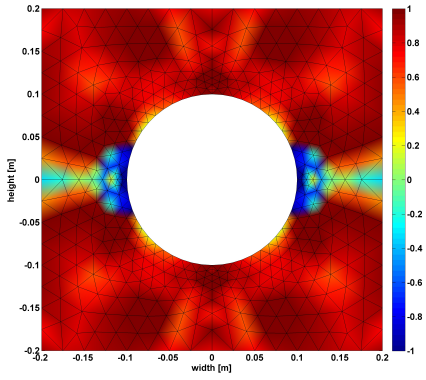

(a) V_1 distribution for optimal stiffness

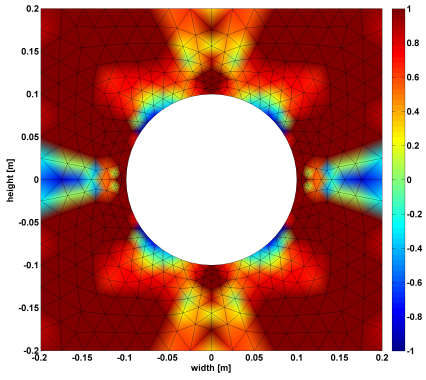

(b) V_3 distribution for optimal stiffness

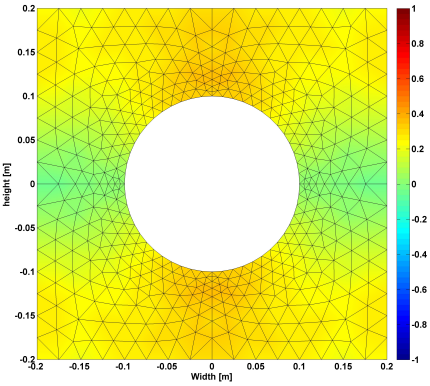

(c) V_1 distribution after fibre angle retrieval step for maximum local steering of $3m^{-1}$

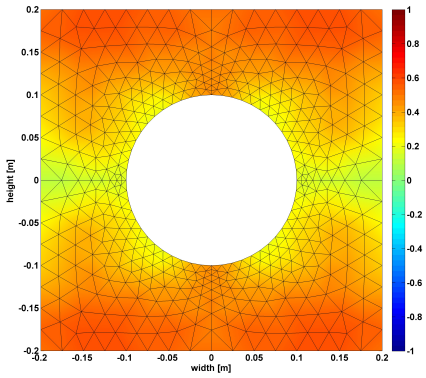

(d) V_3 distribution after fibre angle retrieval step for maximum local steering of $3m^{-1}$

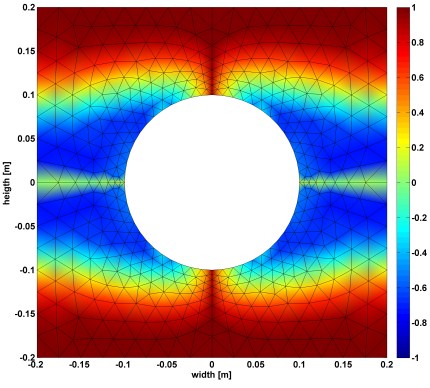

(e) V_1 distribution after fibre angle optimisation for maximum local steering of $3m^{-1}$

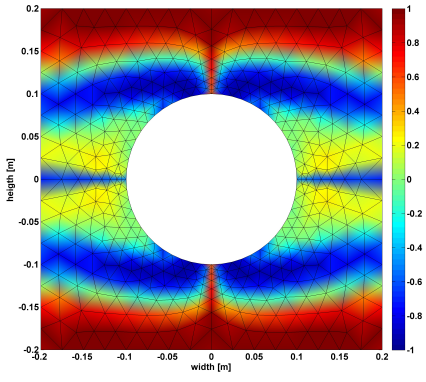

(f) V_3 distribution after fibre angle optimisation for maximum local steering of $3m^{-1}$

Figure 16. in-plane lamination parameters for different cases

Table 6. Overview of the results using different local steering constraints using $3 \cdot 10^{-3}$ as stopping criterion

maximum local steering $[m^{-1}]$	minimum factor of safety after 1 step [-]	optimal factor of safety [-]	number of FEAs	difference w.r.t. optimum after 1 step	difference w.r.t. optimal stiffness distribution	difference w.r.t. tighter convergence criterion
1	1.345	1.688	5	+ 25.5 %	- 13.2 %	- 6.8 %
2	1.357	1.709	5	+ 25.9 %	- 12.1 %	- 6.6 %
3	1.395	1.746	5	+ 25.2 %	- 10.2 %	- 6.6 %

Appendix A. Definition of the lamination parameters

Starting from the general equations for the stiffness matrices [94], using trigonometry, the elements of the stiffness matrix can be rewritten as [95]

$$
\begin{aligned}
\bar{Q}_{11} &= \frac{1}{8}(3\cdot Q_{11}+3\cdot Q_{22}+2\cdot Q_{12}+4\cdot Q_{66})+ \\
&\quad \frac{1}{2}(Q_{11}-Q_{12})\,cos(2\theta)+ \\
&\quad \frac{1}{8}(Q_{11}+Q_{22}-2\cdot Q_{12}-4\cdot Q_{66})\,cos(4\theta) \\
\bar{Q}_{22} &= \frac{1}{8}(3\cdot Q_{11}+3\cdot Q_{22}+2\cdot Q_{12}+4\cdot Q_{66})- \\
&\quad \frac{1}{2}(Q_{11}-Q_{12})\,cos(2\theta)+ \\
&\quad \frac{1}{8}(Q_{11}+Q_{22}-2\cdot Q_{12}-4\cdot Q_{66})\,cos(4\theta) \\
\bar{Q}_{12} &= \frac{1}{8}(Q_{11}+Q_{22}+6\cdot Q_{12}-4\cdot Q_{66})- \\
&\quad \frac{1}{8}(Q_{11}+Q_{22}-2\cdot Q_{12}-4\cdot Q_{66})\,cos(4\theta) \\
\bar{Q}_{66} &= \frac{1}{8}(Q_{11}+Q_{22}-2\cdot Q_{12}+4\cdot Q_{66})- \\
&\quad \frac{1}{8}(Q_{11}+Q_{22}-2\cdot Q_{12}-4\cdot Q_{66})\,cos(4\theta) \\
\bar{Q}_{16} &= \frac{1}{4}(Q_{11}-Q_{12}+)\,sin(2\theta)+ \\
&\quad \frac{1}{8}(Q_{11}+Q_{22}-2\cdot Q_{12}-4\cdot Q_{66})\,sin(4\theta) \\
\bar{Q}_{26} &= \frac{1}{4}(Q_{11}-Q_{12}+)\,sin(2\theta)- \\
&\quad \frac{1}{8}(Q_{11}+Q_{22}-2\cdot Q_{12}-4\cdot Q_{66})\,sin(4\theta).
\end{aligned}
\tag{A.1}
$$

Using these relations, the stiffness matrix of a single layer $\bar{Q}$ can be written as

$$\begin{aligned} \bar{Q} &= \Gamma_0 + \Gamma_1 \cdot cos(2\theta) + \Gamma_2 \cdot sin(2\theta) + \\ &\quad \Gamma_3 \cdot cos(4\theta) + \Gamma_4 \cdot sin(4\theta), \end{aligned} \tag{A.2}$$

with the matrices Γ_i defined as

$$\Gamma_0 = \begin{bmatrix} U_1 & U_4 & 0 \\ U_4 & U_1 & 0 \\ 0 & 0 & U_5 \end{bmatrix} \qquad \Gamma_1 = \begin{bmatrix} U_2 & 0 & 0 \\ 0 & -U_2 & 0 \\ 0 & 0 & 0 \end{bmatrix}$$

$$\Gamma_2 = \begin{bmatrix} 0 & 0 & \frac{U_2}{2} \\ 0 & 0 & \frac{U_2}{2} \\ \frac{U_2}{2} & \frac{U_2}{2} & 0 \end{bmatrix} \qquad \Gamma_3 = \begin{bmatrix} U_3 & -U_3 & 0 \\ -U_3 & U_3 & 0 \\ 0 & 0 & -U_3 \end{bmatrix}, \tag{A.3}$$

$$\Gamma_4 = \begin{bmatrix} 0 & 0 & U_3 \\ 0 & 0 & -U_3 \\ U_3 & -U_3 & 0 \end{bmatrix}$$

where the material invariants U_i are given by

$$\begin{aligned} U_1 &= \frac{3 \cdot Q_{11} + 3 \cdot Q_{22} + 2 \cdot Q_{12} + 4 \cdot Q_{66}}{8} \\ U_2 &= \frac{Q_{11} - Q_{12}}{2} \\ U_3 &= \frac{Q_{11} + Q_{22} - 2 \cdot Q_{12} - 4 \cdot Q_{66}}{8} \\ U_4 &= \frac{Q_{11} + Q_{22} + 6 \cdot Q_{12} - 4 \cdot Q_{66}}{8} \\ U_5 &= \frac{Q_{11} + Q_{22} - 2 \cdot Q_{12} + 4 \cdot Q_{66}}{8}. \end{aligned} \tag{A.4}$$

The A- and D-matrix are calculated using

$$\begin{aligned} A &= \int_{-\frac{h}{2}}^{\frac{h}{2}} (\Gamma_0 + \Gamma_1 \cdot cos(2\theta) + \Gamma_2 \cdot sin(2\theta) + \\ &\quad \Gamma_3 \cdot cos(4\theta) + \Gamma_4 \cdot sin(4\theta))\, dz \\ D &= \int_{-\frac{h}{2}}^{\frac{h}{2}} z^2 (\Gamma_0 + \Gamma_1 \cdot cos(2\theta) + \Gamma_2 \cdot sin(2\theta) + \\ &\quad \Gamma_3 \cdot cos(4\theta) + \Gamma_4 \cdot sin(4\theta))\, dz. \end{aligned} \tag{A.5}$$

Introducing the normalised thickness coordinate

$$\bar{z} = \frac{z}{h}, \tag{A.6}$$

the expressions in eq. (A.5) become

$$\begin{aligned} A &= h \int_{-\frac{1}{2}}^{\frac{1}{2}} (\Gamma_0 + \Gamma_1 \cdot cos(2\theta) + \Gamma_2 \cdot sin(2\theta) + \\ &\quad \Gamma_3 \cdot cos(4\theta) + \Gamma_4 \cdot sin(4\theta))\, d\bar{z} \\ D &= \frac{h^3}{12} \int_{-\frac{1}{2}}^{\frac{1}{2}} \bar{z}^2 (\Gamma_0 + \Gamma_1 \cdot cos(2\theta) + \Gamma_2 \cdot sin(2\theta) + \\ &\quad \Gamma_3 \cdot cos(4\theta) + \Gamma_4 \cdot sin(4\theta))\, d\bar{z}. \end{aligned} \tag{A.7}$$

The lamination parameters are defined as

$$\begin{aligned}
&(V_1, V_2, V_3, V_4) = \\
&\int_{-\frac{1}{2}}^{\frac{1}{2}} \left(\cos\left(2\theta(\bar{z})\right), \sin\left(2\theta(\bar{z})\right), \cos\left(4\theta(\bar{z})\right), \sin\left(4\theta(\bar{z})\right)\right) d\bar{z} \\
&(W_1, W_2, W_3, W_4) = \\
&\int_{-\frac{1}{2}}^{\frac{1}{2}} \bar{z}^2 \left(\cos\left(2\theta(\bar{z})\right), \sin\left(2\theta(\bar{z})\right), \cos\left(4\theta(\bar{z})\right), \sin\left(4\theta(\bar{z})\right)\right) d\bar{z},
\end{aligned} \quad . \tag{A.8}$$